

See discussions, stats, and author profiles for this publication at: <https://www.researchgate.net/publication/263955964>

# Intrinsic Nanoscience of $\delta$ Pu–Ga Alloys: Local Structure and Speciation, Collective Behavior, Nanoscale Heterogeneity, and Aging Mechanisms

ARTICLE in THE JOURNAL OF PHYSICAL CHEMISTRY C · APRIL 2014

Impact Factor: 4.77 · DOI: 10.1021/jp5004038

---

CITATIONS

2

---

READS

25

## 24 AUTHORS, INCLUDING:



Nicolas Bock

Los Alamos National Laboratory

45 PUBLICATIONS 344 CITATIONS

[SEE PROFILE](#)



Takeshi Egami

University of Tennessee

546 PUBLICATIONS 12,177 CITATIONS

[SEE PROFILE](#)



Franz Joseph Freibert

Los Alamos National Laboratory

81 PUBLICATIONS 394 CITATIONS

[SEE PROFILE](#)



Erik Holmström

Sandvik Group

55 PUBLICATIONS 548 CITATIONS

[SEE PROFILE](#)

# Intrinsic Nanoscience of $\delta$ Pu–Ga Alloys: Local Structure and Speciation, Collective Behavior, Nanoscale Heterogeneity, and Aging Mechanisms

Steven D. Conradson,<sup>\*,†</sup> Nicolas Bock,<sup>‡</sup> Julio M. Castro,<sup>§</sup> Dylan R. Conradson,<sup>‡</sup> Lawrence E. Cox,<sup>||</sup> Wojciech Dmowski,<sup>⊥</sup> David E. Dooley,<sup>||</sup> Takeshi Egami,<sup>⊥</sup> Francisco J. Espinosa-Faller,<sup>#</sup> Franz J. Freibert,<sup>†</sup> Angel J. Garcia-Adeva,<sup>§</sup> Nancy J. Hess,<sup>△</sup> Erik Holmström,<sup>‡</sup> Rafael C. Howell,<sup>†</sup> Barbara A. Katz,<sup>||</sup> Jason C. Lashley,<sup>†</sup> Raymond J. Martinez,<sup>†</sup> David P. Moore,<sup>†</sup> Luis A. Morales,<sup>†</sup> J. David Olivas,<sup>†</sup> Ramiro A. Pereyra,<sup>||</sup> Michael Ramos,<sup>†</sup> Jeffrey H. Terry,<sup>||</sup> and Phillip M. Villella<sup>†</sup>

<sup>†</sup>Materials Science and Technology Division, <sup>‡</sup>Theoretical Division, <sup>§</sup>Health, Safety, Radiation Protection Division, and <sup>||</sup>Nuclear Materials Technology Division, Los Alamos National Laboratory, Los Alamos, New Mexico 87545, United States

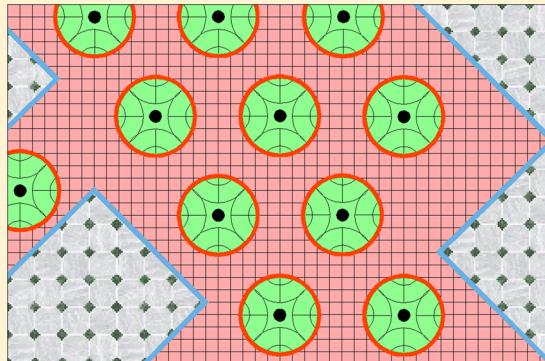
<sup>⊥</sup>Department of Physics and Astronomy, University of Tennessee, Knoxville, Tennessee 37996, United States

<sup>#</sup>Departamento de Física para Ingenieros, Universidad Marista de Mérida, Mérida, Yucatan 97300, Mexico

<sup>△</sup>Departamento de Física Aplicada I, E.T.S. Ingeniería de Bilbao, Universidad del País Vasco, Alda. Urquijo s/n, 48013 Bilbao, Spain

<sup>△</sup>Environmental Molecular Sciences Laboratory, Pacific Northwest National Laboratory, Richland, Washington 99352, United States

**ABSTRACT:**  $\delta$  Pu–Ga alloys and their response to self-irradiation are important scientifically because of the unique complexity of Pu and technologically because of their importance in Science Based Stockpile Stewardship. The local order and structure and the role of the Ga are crucial to understanding the phase stability and the aging effects. X-ray diffraction that gives the long-range average structure of the periodic component of the materials and pair distribution functions analysis and X-ray absorption fine structure that give the overall and the element specific local structure have been used to examine a variety of new and aged materials, including a set of high purity  $\delta$   $Pu_{1-x}Ga_x$  alloys with  $1.7 \leq x \leq 6.4$  atom % Ga that span the low [Ga] portion of the  $\delta$  region of the phase diagram across the  $\sim 3.3$  atom % Ga metastability boundary, a  $\sim 1.7$  atom % Ga alloy that was enriched with  $Pu^{238}$  to accelerate the aging process, and others. We find that metastable alloys contain tens of percents of a novel, “ $\sigma$ ”, Pu structure that we attribute to rearrangement of the Ga-depleted regions after the self-organization of the Ga to form quasi-intermetallic  $Pu_{25-35}Ga$ . This collective and cooperative behavior involving the Ga and other defects in terms of a tendency to aggregate into domains with structures that differ from the  $\delta$  host and the resulting nanoscale heterogeneity also appears to play an important role in the observation of analogous locally ordered structures in aged materials. This description of these materials and their aging is radically different from current conceptual basis derived from other experiments that are insensitive to ordering on the angstrom–nanometer length scale.



## INTRODUCTION

Because short wavelength X-ray and neutron diffraction are sensitive only to the long-range average arrangement of the atoms in the coherent portion of a crystal, complementary local structure measurements are required for a complete understanding of the structure of a complex material.<sup>1–7</sup> This is particularly an issue in solid solutions where even a random distribution of a solute will result in nanometer-scale fluctuations in the local composition. Such fluctuations are greatly enhanced if the solute (or charge or spin or defect) distribution is organized by collective and cooperative phenomena. These occur in the form of interactions between these inhomogeneities that control or at least influence their placement relative to each other to give static (with solutes or

defects) or dynamic (with itinerant charge or spin) (quasi-)ordered structures. One consequence of this solute clustering would be that, when the local composition of sets of atoms deviates from the average enough to fall outside the phase boundaries of the bulk material, there would reside within the crystal domains that would be unstable in the structure of the host phase if they stood alone. If the tendency of these atoms to rearrange their structure as dictated by their phase diagram is greater than the pinning effect exerted by their host, then they may rearrange to form embedded domains at or below the

Received: January 13, 2014

Revised: March 20, 2014

Published: March 24, 2014



diffraction limit in size, resulting in a phase-separated, heterogeneous material.<sup>3,5–9</sup> The atoms in these domains could shift into the structure expected from their phase diagram, e.g., nanoscale Fe in or on Cu,<sup>10–13</sup> but could also easily assume novel “structures”—a lighter term than “phase” appropriate to their small sizes and existence only within or on the surface of another compound—engendered by effects accruing to this phenomenon such as epitaxial and tensile stress. This coupling over multiple length scales between the atomic scale ordering (or lack thereof) of inhomogeneities in the lattice and defects, elastic forces, phase competition, and texture in the form of coexisting structures is a hallmark of martensites,<sup>14–26</sup> a class of complex materials that includes  $\delta$ -stabilized Pu–Ga.

The development of accurate predictive models for Pu and its alloys is one of the central issues of Science Based Stockpile Stewardship (SBSS). With the closure of the weapons production facilities and the moratorium on nuclear testing, SBSS is the primary means for ensuring the reliability of the U.S. stockpile.<sup>27,28</sup> In addition to the conventional issues of, e.g., corrosion, phase stability, etc., Pu has the additional problem that its self-irradiation continuously changes its composition and introduces defects that increase its internal energy.<sup>29–36</sup> Models of Pu must therefore be aimed at a target that not only is arguably one of the most complicated of all the elements but also is moving.

The enigmatic and extreme nature of Pu<sup>37–40</sup> includes six crystallographic phases at ambient pressure prior to melting. These begin with the high density, monoclinic  $\alpha$  phase that is stable through room temperature and pass through the fcc  $\delta$  phase that exhibits a 25% lower density and a negative thermal expansion coefficient. The critical parameter in the enthalpy is the spatial extent of the f orbitals. For elements below Pu in the actinide row these are expanded and bonding, pulling the atoms together. Above Pu they are localized and nonbonding to give low density structures. But Pu, at the cusp, is ambivalent and displays both behaviors. The narrowness of the f band and its tight correlation with such radical changes in structure sensitizes Pu to strong coupling of its structure to other competing components of its total free energy.<sup>38–40</sup> The crucial metallurgical issue has therefore been finding elements that stabilize the ductile  $\delta$  phase to ambient temperature so that the resulting alloys can be formed precisely.<sup>40</sup> Ga is the most widely used addition for this purpose, stabilizing or retaining  $\delta$  Pu starting as low as around 1 atom % with careful homogenization and going as high as just over 10 atom % before the intermetallic Pu<sub>3</sub>Ga begins to separate.

The mechanism by which Ga,<sup>41,42</sup> as well as Al, In, Sc, Am, Ce, Zn, etc., stabilizes the  $\delta$  phase is still a mystery. This may be largely because consensus on the mechanism by which the  $\delta$  phase itself is stabilized is lacking despite its status as its own scientific industry,<sup>43–72</sup> although recently there may be some experimental and theoretical convergence that its properties may be best explained by the ground state being a combination of several different electronic configurations.<sup>54,73–75</sup> Some of these elements are larger than Pu and some smaller, some trivalent and some not, some more electronegative than Pu and others more electropositive. Nor do they simply shift the phase diagram. The martensitic transformation of  $\delta$  Pu for alloys with concentrations of the alloying element that stabilize the  $\delta$  phase below the metastability limit where the transformation temperature is still greater than 0 K converts up to a few dozen percent of the material directly into ten to hundred

micrometer size grains of the  $\alpha'$  phase ( $\alpha$  Pu that contains the original alloy element as an impurity), bypassing the  $\beta$  and  $\gamma$  phases, a process that is reversed at around 400 K.<sup>76–81</sup>

These behaviors pose the question of how Pu alloys are best considered. A mean-field physics-type approach that averages the properties of the individual atoms into a homogeneous crystal is consistent with phase stability being a bulk thermodynamic property. In this kind of description the mechanism could simply be a decrease in the relative strength of the f bonding so that the factors stabilizing the  $\delta$  phase, e.g., the vibrational entropy of the fcc structure and the exact form of the spin–orbit coupling, become more important at lower temperatures.<sup>82–85</sup> The available structural evidence, however, points instead to localization, meaning that the adatom retains much of its original elemental identity and that its influence on the Pu atoms diminishes rapidly with increasing distance from the atom in the second, third, etc. neighbor shells. The material will therefore lack structural homogeneity on the atomic scale by exhibiting lattice distortions around the adatom. Not only are there relatively large differences between Pu–Pu and Pu–X bond lengths that must be accompanied by significant elastic strain<sup>8,9,86–93</sup> but also these different bonds can display widely varying Debye temperatures.<sup>90,94</sup> Localization suggests a more “chemistry” type of approach in which the atoms are best considered as distinct chemical species even within a metallic milieu, with clusters of atoms as the basis for their electronic structure rather than a periodic lattice. Chemistry as opposed to physics would also favor nanoscale heterogeneity,<sup>3,5–7,95</sup> the aforementioned organization of inhomogeneities and fluctuations in local composition to give multiple, coexisting, ordered structures with the minor one(s) occurring as domains within host lattice that are at or below the diffraction limit in size. It is thus consistent with Pu alloys exhibiting unusual structural behavior of this type, including the possibilities of coexisting ordered structures in  $\delta$ -stabilized Pu–Ga and enhanced homogeneity on aging that have been suggested based on earlier extended X-ray absorption fine structure (EXAFS) spectroscopy and X-ray pair distribution function (pdf) measurements.<sup>8,9,27,28</sup> Measurements on a defined set of laboratory-prepared materials made from ultrapure Pu now unequivocally demonstrate this heterogeneity in newly prepared metastable alloys while results from aged samples demonstrate the importance of the heterogeneity in aging processes in Pu. These findings also pose the question of whether these behaviors are specific to Pu or are instead an attribute common to the broader class of complex functional materials such as stripes in mixed valence correlated transition metal oxides,<sup>20,96–100</sup> most of which also display inhomogeneities in the form of bulk compositions and/or charge distributions at variance with the stoichiometries of their unit cells.

## MATERIALS AND METHODS

**Preparation and Characterization of Samples.** A set of Pu–Ga alloys (Pu is a serious radiation and chemical hazard that can only be handled in special facilities) containing 1.7, 2.3, 3.0, 3.7, 4.7, and 6.5 atom % Ga (composition confirmed by lattice parameters determined by laboratory based XRD) were prepared by arc-melting Ga with zone-refined Pu and rolling pieces into thin foils that were then homogenized at 450 °C for 48 h. (The Pu<sub>0.983</sub>Ga<sub>0.017</sub> sample was annealed twice for 24 h each time for the same total time because some traces of  $\alpha$  Pu were still observed after the first heating.) At that time no traces

of the diffraction pattern of  $\alpha$  Pu could be found in the  $\text{Pu}_{0.983}\text{Ga}_{0.017}$  sample that would have been most susceptible to its formation because of the uneven distribution of Ga within the grains, known as “coring”, that the annealing process eliminates. A 2.7 atom % Ga sample was made from electrorefined Pu and homogenized for 200 h (lattice parameter also confirmed by laboratory based XRD). This sample is included here because, although prepared from somewhat less pure starting material (higher concentrations of other trace elements but lower uranium) and homogenized differently, it is nevertheless well characterized and understood and gave the best pair distribution function of any material because, fortuitously, it was less textured. Although for the most part discussed separately from the aged materials, we will call these samples “new” to distinguish them from the others. Sample integrity was also confirmed by extensive diffraction measurements on several samples at the synchrotron across a temperature range of 30–150 K. The ca. 1.7 atom % Ga accelerated aging project (AAP)<sup>33</sup> was made from material originally possessing a typical isotopic distribution (>90%  $^{239}\text{Pu}$ ) to which  $^{238}\text{Pu}$  was added so that its  $\alpha$  self-irradiation rate was accelerated by a factor of >10. Ages for this material are reported as the number of years that a normal sample would require for the same number of  $\alpha$  disintegrations. These and other aged samples were cut from billets with a diamond saw. Laboratory based XRD that confirmed the compositions via the lattice parameters was performed on the AAP and several other aged samples. The surfaces were prepared and sample thicknesses reduced to around 100–150  $\mu\text{m}$  by hand polishing, followed by electropolishing to remove any surface oxide and  $\alpha$  Pu that forms in response to the uniaxial stress of the polishing operation. Synchrotron XRD was performed on several samples. The lower resolution diffraction pattern (as  $S(Q)$ ) from a pdf scan of the 3.0 atom % Ga sample at 90 K using 35,000 eV X-rays is shown in Figure 1 as a representative diffraction pattern for all of these materials.

**Acquisition and Analysis of XAFS Spectra.** Pu samples were loaded into specially designed holders in which the probed surface was not in contact with any organic material in gloveboxes within the Los Alamos Pu facilities and triply contained at all times afterward. All operations were performed using procedures developed by this group in conjunction with the synchrotron laboratories’ safety teams that include ventilation of the experimental hutches through HEPA filters and the use of continuous air monitors. Experimental measurements were performed at the Stanford Synchrotron Radiation Laboratory on end stations 4-2, 7-2, 10-2, and 11-2 and the Advanced Photon Source at the MR and PNC Collaborative Access Team beamlines. The Si [220] monochromator crystals were fully tuned with harmonic rejection for XAFS accomplished with a flat, Pt-coated mirror tilted to have a cutoff energy of 21–25 keV for Pu and 13–15 keV for Ga. The energy was calibrated by defining the first inflection point of a Zr foil as 17999.35 eV, which puts the inflection point of the Pu edge at 18056.7–18057.0 eV. Useful EXAFS spectra were obtained near 35 and 85 K because the Debye temperature of  $\delta$  Pu is only around 100 K. Not all samples were measured at all temperatures, most notably, the Ga XAFS of the 2.3, 2.7, and 4.7 atom % Ga samples were not measured at 35 and 90 K because of exigencies of beam time and the fact that many other samples measured previously had not (as these data corroborate) exhibited any Ga concentration (we will use the chemistry shorthand,  $[\text{Ga}]$ ) dependence. In retrospect these

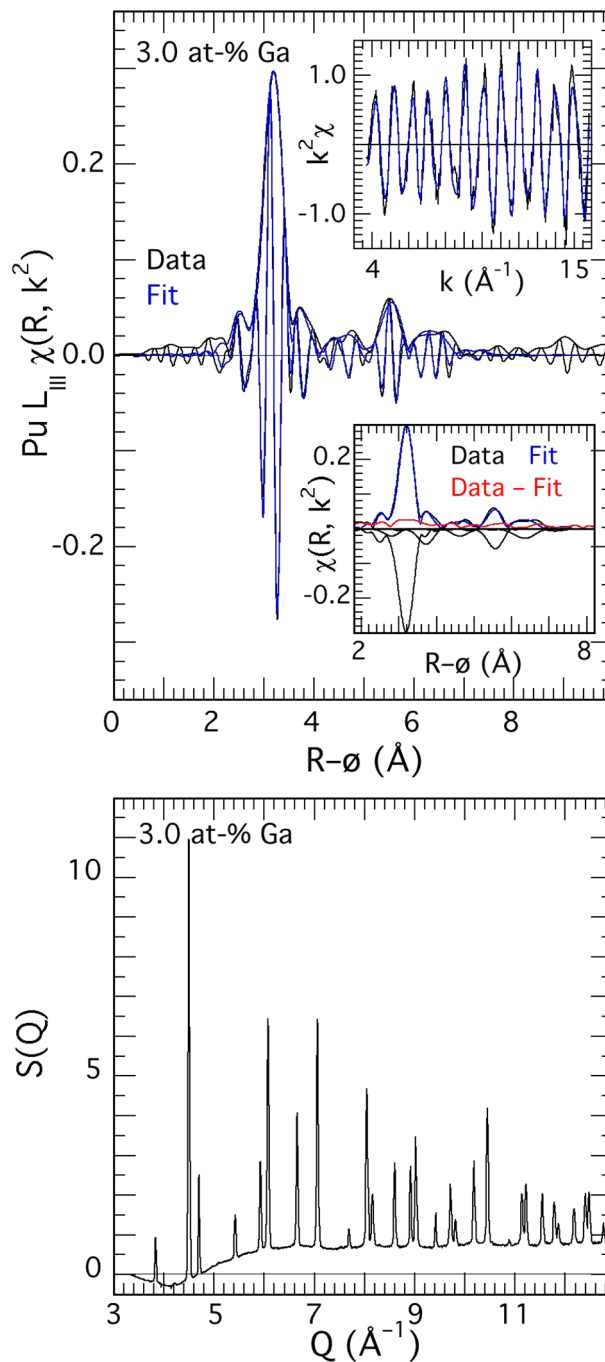


**Figure 1.** (Upper) The moduli and real components of  $\chi(R, k^2)$  (=Fourier transform of  $(k^2 \chi(k))$ ) vs  $R$  that is uncorrected for the phase shift (thus,  $R - \phi$ ) for the Pu L<sub>III</sub> data and fit of  $\text{Pu}_{0.970}\text{Ga}_{0.030}$  at 35 K. Insets show (upper) this same curve fit in  $k$  space and (lower) the moduli only of the data, fit, and difference together with the individual contributions of each shell in the fit (inverted). (Lower)  $S(Q)$  of this sample measured at 90 K at the synchrotron as a representative diffraction pattern of these new Pu–Ga samples. The background for the  $S(Q)$  function is typical of the reflection geometry and material.

omissions were unfortunate, but because of the complexity and expense of these experiments they cannot be repeated. The credibility of these results, however, is validated not only by their consistency with respect to each other but also because they reproduce prior observations on a large number of other samples.<sup>93</sup> Ambient temperature measurements were also made prior to cooling for many samples. The temperature-induced

martensitic transformation to  $\alpha$ - $\delta$  mixtures has *not* been observed in EXAFS<sup>8,86–92</sup> or X-ray/neutron<sup>101,102</sup> scattering measurements on such samples, including those presented here, although broadening of the Bragg peaks does occasionally occur. Other types of measurements such as dilatometry and electron microscopy, however, have found evidence for complicated transformational behavior extending to very low temperatures<sup>47,103,104</sup> that therefore, by definition, involve the formation of poorly or nondiffracting domains associated with the retained  $\delta$  precursor and host. Comparison with the ambient temperature spectra indicates that cooling of the samples for XAFS did not affect the results reported here. EXAFS measurements were made in the fluorescence mode with multielement Ge detectors with digital amplifiers for the new and most aged samples and occasionally with an ionization type detector. Dead time errors were minimized by maintaining maximum count rates of <120 kHz for each channel to keep the live times >90%, but the resultant reduction in amplitude of a few % was also corrected in the analysis using a 1.5  $\mu$ s dead time. Samples were >100  $\mu$ m thick to avoid possible artifacts in the material that could result from fabricating thinner, transmitting Pu foils. The spectra of fully absorbing samples are more sensitive to beam noise, which explains the perhaps unexpected amount of high frequency noise displayed. Since the self-absorbance correction is identical for all samples (the decrease in Pu concentration is apparently almost exactly compensated by the decrease in lattice parameter with higher [Ga] while the Ga self-absorption is negligible to minimal because of its low concentrations), direct comparisons of identically corrected or uncorrected spectra are valid. Most scattering measurements, including all pdfs, were performed in reflection geometry at 18 and 33 keV; diffraction measurements on AAP samples at 22 equivalent years were made in transmission geometry at 75 keV. XAFS and X-ray pdf data were analyzed by methods described in detail for other systems, with great care taken in the analysis and especially the EXAFS normalization and background subtraction to use very similar parameters for all spectra so that differences between them cannot be analysis artifacts. One instance that was found, a beam fluctuation caused by a discontinuity in the Ga edge of a sample at ambient temperature, is noted in the figure that contains this spectrum. The EXAFS were calculated as the difference between the full spectra and their smooth atomic backgrounds approximated by an arctangent and Gaussian for the edge and a polynomial spline at higher energies, divided by the atomic absorbance fall off with increasing energy. The locations of the spline knots were varied to minimize the modulus area below  $R = 2 \text{ \AA}$ , with the locations constrained to be within a few tenths of an  $\text{\AA}^{-1}$  of the average position for all spectra. The curve-fit and Fourier transform ranges for spectra measured at 35 K are  $k = 3.70\text{--}15.85 \text{ \AA}^{-1}$  ( $E_0 = 18058 \text{ eV}$ ) for Pu and  $3.50\text{--}13.50 \text{ \AA}^{-1}$  ( $E_0 = 10731 \text{ eV}$ ) for Ga, at 90 K are  $k = 3.70\text{--}13.75 \text{ \AA}^{-1}$  for Pu and  $3.50\text{--}13.50 \text{ \AA}^{-1}$  for Ga, and at ambient temperature where higher noise levels were acceptable because curve fits were not performed (~298 K) are  $2.65\text{--}14.00 \text{ \AA}^{-1}$  for Pu and  $2.50\text{--}13.00 \text{ \AA}^{-1}$  for Ga. Ripple in the Fourier transforms was minimized (at the expense of some peak broadening) by applying a sine window to the spectra prior to the integration. The fact that the amplitude of the FT is tremendously affected by the window function and many different functions are used by different groups must be taken into account in comparing these data with others. The scales in Figures 1 and 2, Figures 3 and 4, Figures 5, 6, and 11, and

Figures 10 and 13 are identical so that direct comparisons of spectra in figures can be made within this report.

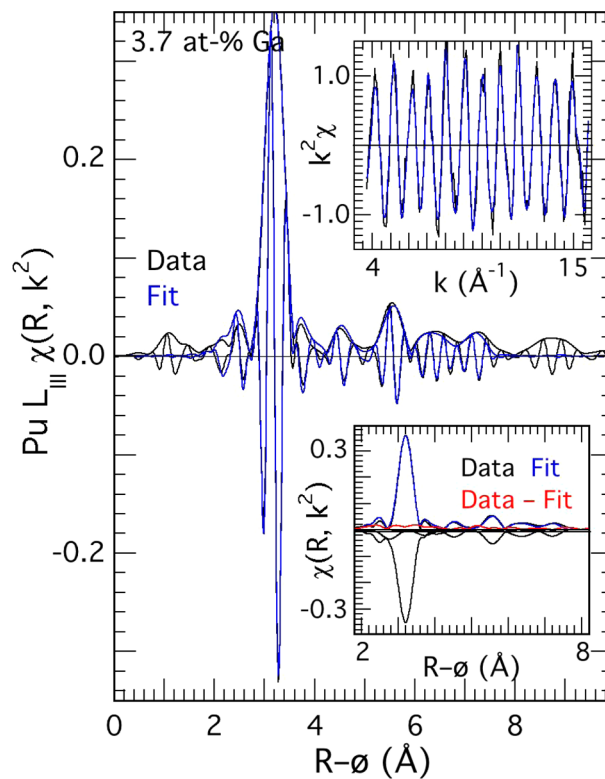


Figure 2. Same as Figure 1, but for  $\text{Pu}_{0.963}\text{Ga}_{0.037}$  at 35 K.

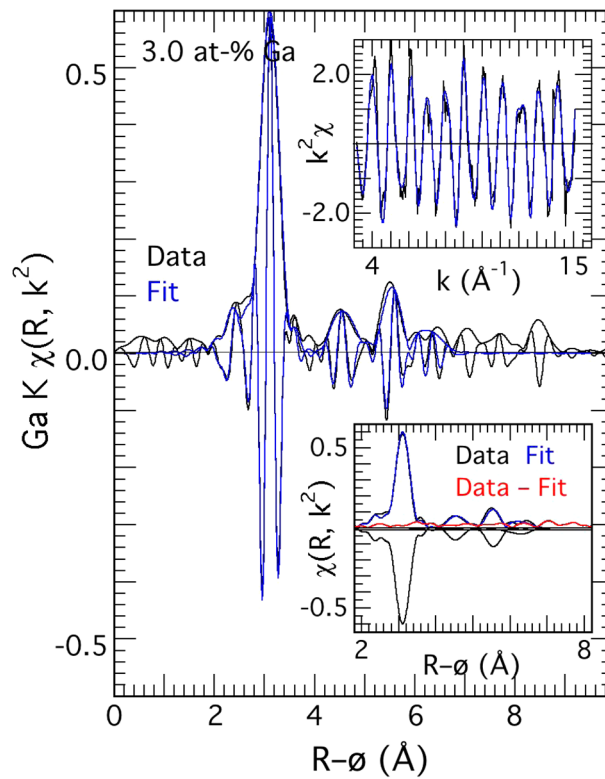
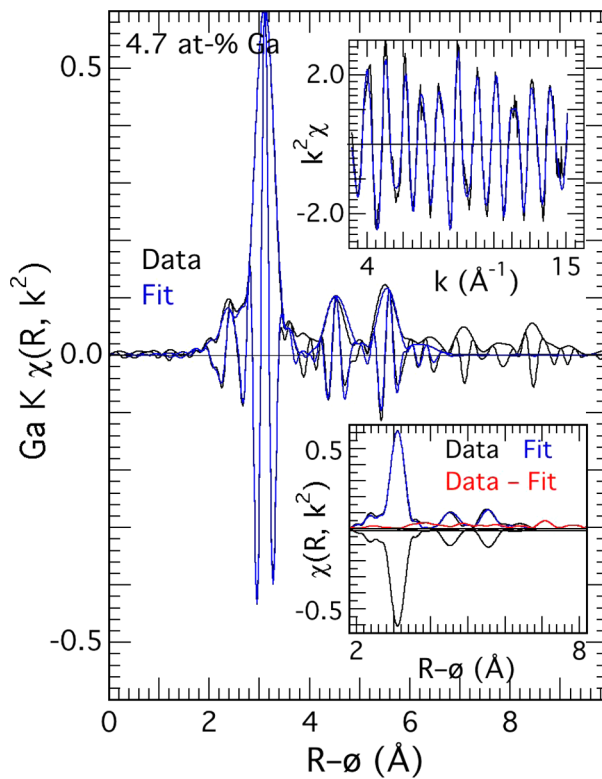


Figure 3. Same as Figure 1, but for the Ga K EXAFS of  $\text{Pu}_{0.970}\text{Ga}_{0.030}$  at 35 K.



**Figure 4.** Same as Figure 1, but for the Ga K EXAFS of  $\text{Pu}_{0.963}\text{Ga}_{0.037}$  at 35 K.

Curve fits using amplitudes and phases calculated with the FEFF code<sup>105</sup> allowed the number of atoms ( $N$ ), some  $\sigma$ 's (the Gaussian width of the pairwise harmonic distribution), and the interatomic distances ( $r$ ) to float, with the  $\Delta E_0$ s constrained to be equal for all shells and typically constrained and fixed  $\sigma$  values for the more distant shells to obtain reasonable values for  $N$ .  $\chi(k)$  curve fits and their corresponding  $\chi(R)$  representations are shown for the two of the Pu and two of the Ga spectra from the new samples at 35 K (Figures 1–4); all others are of similar quality. However, metrical parameters obtained from curve fitting are not used in the interpretation, with the exception of some of the distances, because verifying well documented crystallographic parameters is not the objective of this work.

## RESULTS AND DISCUSSION

The goal of these combined EXAFS-pdf-xrd measurements is 2-fold. The first goal is to identify and characterize collective behavior and the resultant nanoscale heterogeneity in terms of, respectively, Ga clustering and the rearrangement of the Pu atoms in the Ga-depleted regions into  $\sigma$  Pu,<sup>3,9,36,106</sup> a novel structure that may be  $\alpha$  Pu under tensile stress, via a set of newly prepared  $\delta$ -stabilized Pu–Ga alloys. The second objective is to determine if this cooperativity is a general phenomenon in  $\delta$  Pu that would make it relevant to its response to its self-irradiation or if the damage is adequately described by the conventional approach that assumes weak interactions between the radiation-induced defects.<sup>36</sup> As this report (and another<sup>93</sup>) describes, these local structure measurements demonstrate that in Pu–Ga the Ga self-organizes to form a quasi-intermetallic of composition  $\text{Pu}_{25–35}\text{Ga}$  instead of forming a random solid solution. As postulated before from a variety of samples<sup>8,9</sup> and in part now corroborated by two other groups,<sup>36,106</sup> prior to saturation of the material at around 3.3

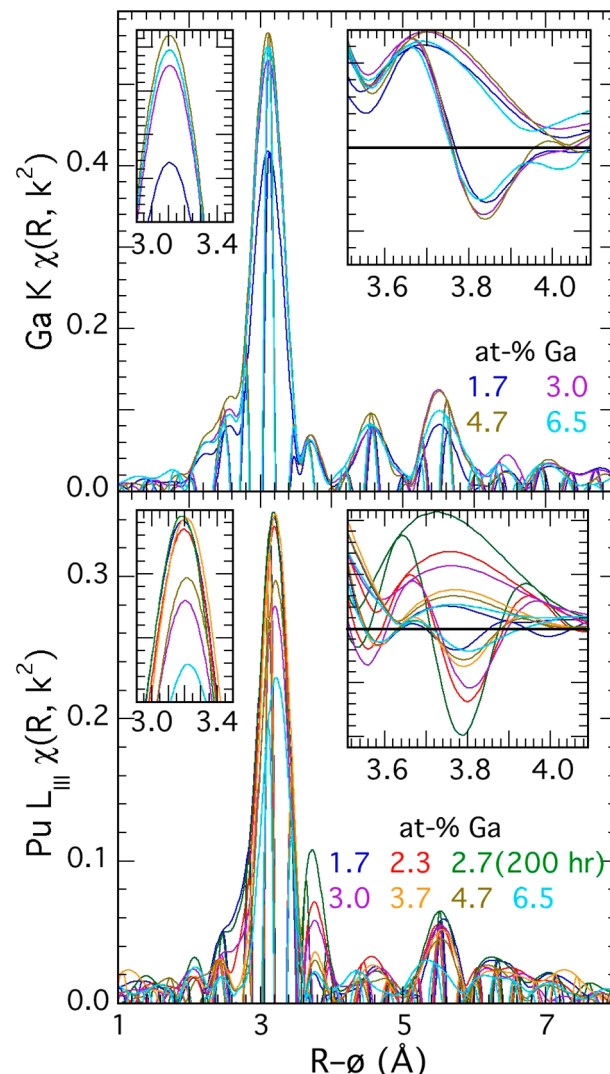


**Figure 5.** The modulus and real component of  $\chi(R, k^2)$  (= Fourier transform of  $(k^2\chi(k))$ ) vs  $R$  that is uncorrected for the phase shift (thus,  $R - \phi$ ) for the new Pu–Ga alloys at 35 K. The upper plot contains the Ga EXAFS; the lower is the Pu EXAFS. Insets show the primary peak modulus (left) and the feature that is variable with [Ga] (right) in the Pu spectra but displays no change for Ga.

atom % Ga with this ordered compound, the nanoscale Ga-depleted and consequent Ga-excess domains rearrange within the  $\delta$  lattice into a structure (or structures) different from the fcc one of their host. Using the same type of analysis that characterized the heterogeneity and nanophasse separation in new materials, we find that this type of process is also active for the radiation-induced defects accompanying aging.

**Analysis and Interpretation of EXAFS Spectra.** Within this context of elucidating the heterogeneity rather than simply extracting metrical parameters for a homogeneous material as it disorders, the analysis problem is therefore different, obviating a simple curve-fitting approach. Structural characterization of disordered materials is challenging, and understanding radiation effects that increase or modify the disorder is even more so. Evaluating disorder requires separating harmonic-like from anharmonic-like effects on the individual waves from the various neighbor atom shells that constitute the absorber–scatterer pairs. Harmonic disorder increases the widths of the peaks in the distributions and causes energy-dependent

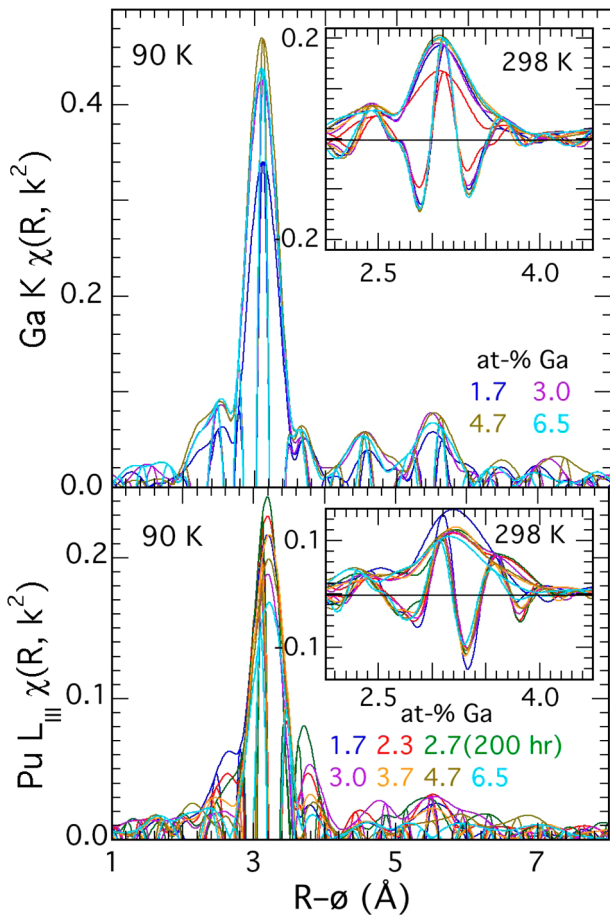


**Figure 6.** The modulus and real component of  $\chi(R, k^2)$  for new Pu–Ga alloys at 90 K and (insets) at ambient temperature prior to cooling. The upper plot contains the Ga EXAFS; the lower is the Pu EXAFS. The red and orange spectra in the Ga EXAFS at 298 K are from, respectively,  $\text{Pu}_{0.977}\text{Ga}_{0.023}$  and  $\text{Pu}_{0.963}\text{Ga}_{0.037}$ . The Ga EXAFS of  $\text{Pu}_{0.977}\text{Ga}_{0.023}$  at 298 K displays diminished relative amplitude only at this temperature because of a beam deviation within the absorption edge that affected normalization.

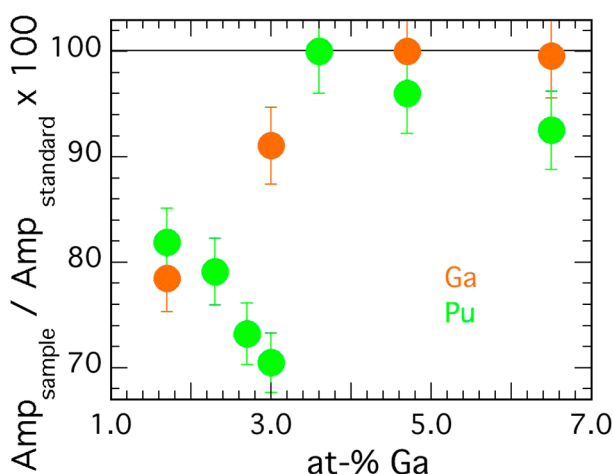


**Figure 7.** The percent of atoms in the Pu (green) and Ga (orange)  $\delta$  nn shell relative to those found for the standard (the 3.7 atom % Ga for Pu and 4.7 atom % Ga for Ga) samples as a function of [Ga] for the newly prepared samples. Uncertainties in the calculation, estimated by altering the parameters used in the calculation of these values, are  $\leq 4\%$ .

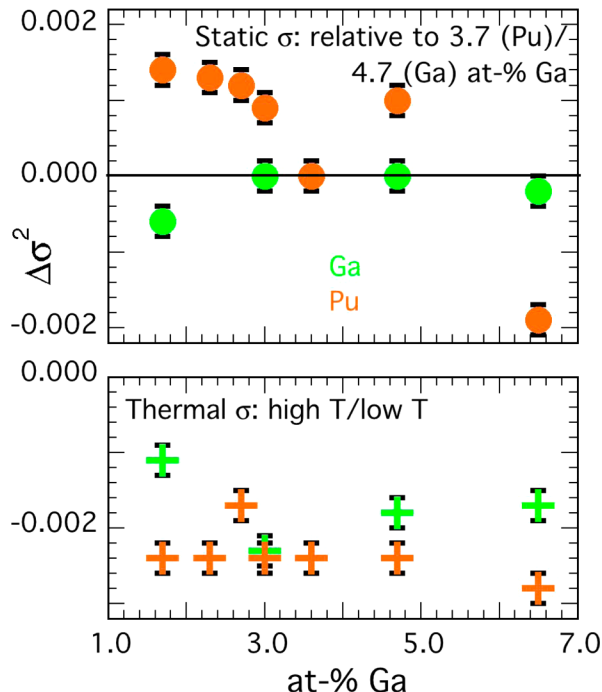


**Figure 8.** Upper: The difference in the nn Debye–Waller factor of the indicated sample and Pu–Pu or Pu–Ga bond relative to the 3.7 (for Pu, orange circles)/4.7 (for Ga, green circles) atom % Ga basis spectra for indicated samples as a function of [Ga] calculated by the logarithm–amplitude ratio method. Numbers >0 in the upper plot of the static component indicate that the Deybe–Waller factor of the material is smaller than that of the basis one. Lower: Differences in the Debye–Waller factor between 35 and 90 K, also calculated as logarithm–amplitude ratios of the upper temperature divided by the lower. The uncertainties in the calculation, estimated by repeating it using different background parameters and curve fits, are  $\leq 0.0002 \text{ Å}^2$ .

damping of the EXAFS waves. Anharmonic disorder splits or otherwise complicates the peaks in the distributions and causes, in addition to the damping, a reduction in the amplitude of the EXAFS waves even in the low  $k$  region where the number of atoms in the neighbor shells giving each wave is derived by extrapolating the curve fit. The application of EXAFS to study disorder in  $\delta$  Pu alloys is afflicted with two more problems specific to this system. The first is that this separation of the number of atoms in a neighbor shell ( $k = 0$  amplitude) from the effects of the shape of the distribution within the shell (damping) is unusually difficult for Pu because its back-scattering amplitude is relatively low at low  $k$  and is disrupted around  $k = 4 \text{ Å}^{-1}$  by a Ramsauer–Townsend resonance that is difficult to calculate accurately. The second is that  $\delta$  Pu alloys often exhibit the aforementioned nanoscale heterogeneity,<sup>3</sup> i.e., multiple, coexisting, ordered structures within the same crystal in which the domain sizes of the minority structure are at or below the diffraction limit in size, so that an essential portion of the analysis must be identifying and separating the spectral contributions of the second structure from the principal one. This poses a dilemma for characterizing radiation effects. One approach is to do so within the classical model in which the accumulation of point defects disrupts the long and then medium range order in the material that eventually becomes amorphous. In this case the principal question is how rapidly this sequence of events occurs as dictated by the rate of self-annealing and whether it results in the formation of voids and subsequent swelling of the material. The alternative that is

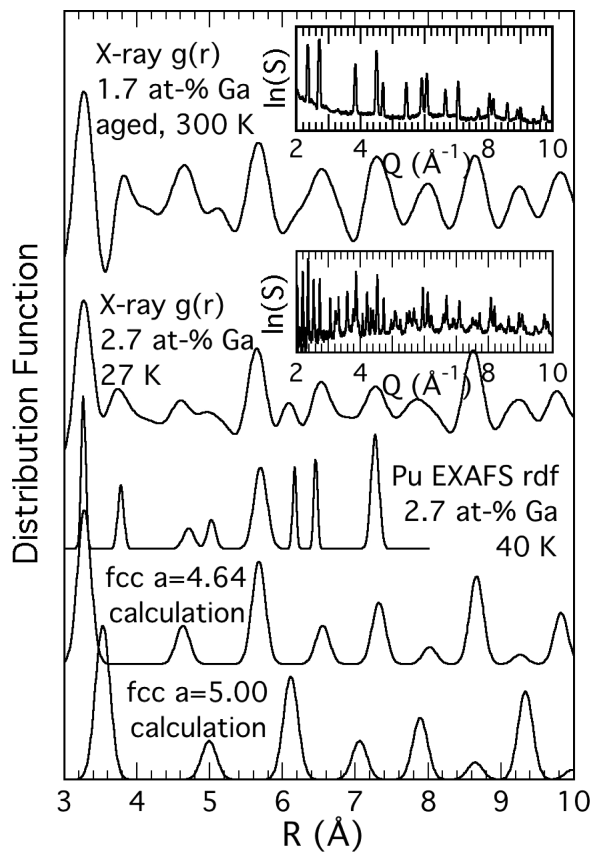


**Figure 9.** Pu  $g(r)$ /partial pair distribution function for indicated samples and methods,  $\ln(S(Q))$  from which the two  $g(r)$  functions were calculated, and (lower two) pair distribution functions calculated from the  $\delta$  and a larger fcc structure that represents the  $\sigma$  structure beyond the first shell that appears to be split by a structural modulation. The top two X-ray  $g(r)$  functions were obtained directly by Fourier transformation of the measured  $F(Q)$  function for  $Q = 1.5\text{--}22 \text{\AA}^{-1}$ ; the EXAFS  $g(r)$  was calculated from curve-fit results.  $S(Q)$  is presented as the logarithm to emphasize the opposite behavior of the  $\sigma$  diffraction pattern in the two samples despite the similarity of their  $g(r)$ 's.

important in a heterogeneous or inhomogeneous complex material and the topic of this report is the extent to which the energy distributes itself in specific ways. An example is our observations on the U and other elements in glass,<sup>107</sup> preferentially breaking or rearranging certain bonds and even an aggregation of the defects that alters the local composition and causes the rearrangement of the atoms in these domains to form novel structures.

The critical factor in the analysis for determining if other structures have formed in response to internal elastic stress from the intrinsic defects, e.g., the Ga, or from the radiation-induced ones is therefore not the Debye–Waller factor but the number of atoms in a particular neighbor shell. Given the problems just described in separating these two components of the EXAFS amplitude, we obtained the most consistent results by a somewhat unconventional method that is nevertheless equivalent to standard curve fitting but more accurate because it focuses on the low energy region of the EXAFS before its amplitudes are significantly modified by disorder-induced damping and it is unaffected by inaccuracies in the calculated amplitudes and phases. Curve fits guided by and consistent with the results presented were performed on all spectra, with

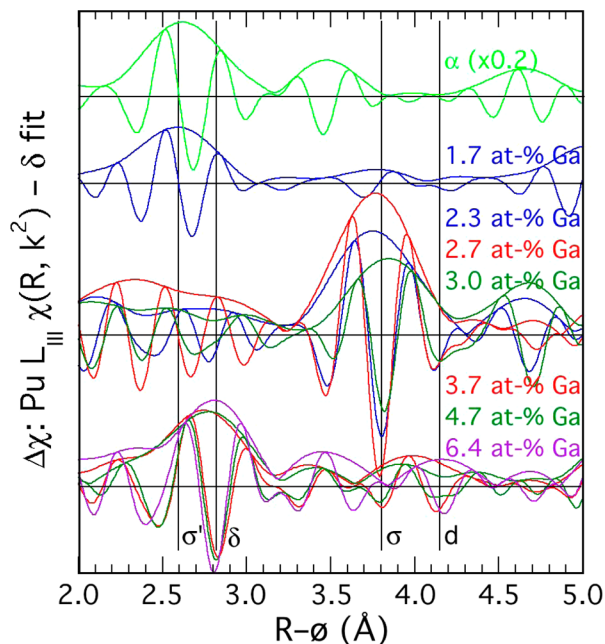


**Figure 10.** Pu  $\chi(R, k^2)$  residuals obtained by subtracting the curve fit with only the  $\delta$  shells of atoms from the spectra from  $k = 3.7\text{--}14.8 \text{\AA}^{-1}$ . The lines act as approximate guides to features exhibited by several spectra that are associated with the  $\sigma$  and  $\sigma'$  structures, and the  $\delta$  structure, as well as initial radiation damage in 1.7 atom % Ga materials (d, see Figure 13) and radiation-damaged structures that do not occur in these new samples. The real component minimum occurring at the maximum of the modulus for the  $\sigma$  and  $\delta$  features is the pattern expected for a simple Pu shell. A spectrum of  $\alpha$  Pu reduced in amplitude by a factor of 5 is included with those of the new samples for comparison with the  $\sigma'$  feature, which in  $\alpha$  Pu is produced by a complex Pu distribution.

special attention paid to how well the calculated Pu–Pu or Ga–Pu waves fit the spectral features of interest as the criterion for whether or not a spectral feature was indicative of a corresponding non-fcc  $\delta$  structural one in the material. These fits therefore gave metrical parameters to check against other spectra. More importantly, they were also used to isolate the contributions from the individual neighbor shells in the material, both those belonging to the  $\delta$  phase and those from other structures, by subtracting from the data all of the waves composing the fit except for the contribution of the shell of interest. The amount of  $\delta$  phase was then obtained from the area of the wave from the nearest neighbor (nn)  $\delta$  shell around  $3.28 \text{\AA}$ . This was done by fitting a fourth order polynomial to the normalized spectrum over the range  $E_0+19\text{--}187$  for Pu and  $E_0+11\text{--}174$  eV for Ga (energies were selected to use nodes as the end points), subtracting this polynomial to obtain the low  $k$  EXAFS spectrum, subtracting the contributions of all of the other shells found by the curve fit over the full range, and summing  $|\chi(k)|$  in the range  $k = 2.36\text{--}4.96 \text{\AA}^{-1}$  for the Pu and  $2.00\text{--}5.00 \text{\AA}^{-1}$  for the Ga spectra. This number was converted to a relative quantity by dividing it by the value from the 3.7 atom % Ga spectrum for Pu and the 4.7 atom % Ga spectrum for Ga that were measured at the same temperature and that are expected to have the greatest fraction of  $\delta$  Pu, at or closest to 100%. These values, expressed as the percent  $\delta$  phase present in the material relative to  $\text{Pu}_{0.963}\text{Ga}_{0.037}$  (Pu) and  $\text{Pu}_{0.953}\text{Ga}_{0.047}$  (for Ga), are the basis for Figures 7 and 12. The relative numbers of atoms obtained from curve-fit and logarithm-ratio

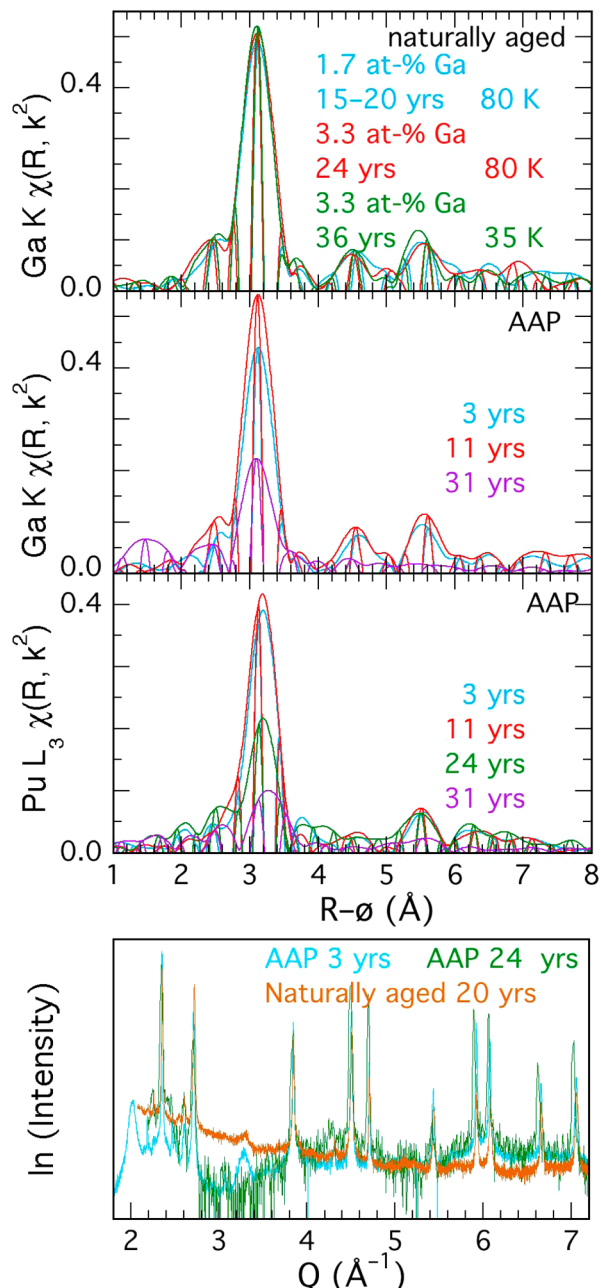


**Figure 11.** Upper:  $\text{Ga K}\chi(R)$  for naturally aged and Ga and Pu  $\chi(R)$  for AAP samples. Lower: Synchrotron XRD patterns for selected aged samples. Age of AAP samples is in “equivalent years”, derived from its activity relative to that of standard Pu.

analyses gave identical trends with somewhat greater variation in the actual values. Based on the effects of variations in the end points and other parameters and comparisons with curve fits and logarithm-ratioing, uncertainties in these values are mostly  $\leq 4\%$  with a few outliers of 6–9% in the aged samples that displayed the most disorder, lowest spectral amplitudes, and highest probability of anharmonic distributions. Changes in the Debye–Waller factors as in Figures 8 and 14 were obtained directly using the logarithm-amplitude ratioing method that has the advantage over curve fitting in that it reveals problems when the ratio is only poorly linear that are often not apparent in curve fits and also that errors can be calculated as the least-squares difference between the actual ratio and the line fit to it.

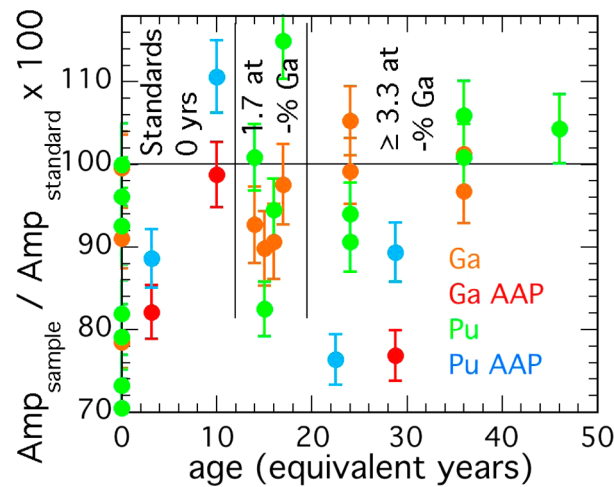


**Figure 12.** Same as Figure 7 but as a function of age. The standard for Pu is the 3.7 atom % Ga new sample, for Ga the 4.7 atom % Ga new sample. The results from the new materials are placed on zero years. The abscissa refers to the actual age for naturally aged samples and the equivalent age based on the higher specific activity because of the Pu-238 in the AAP samples, which are shown in red (Ga) and blue (Pu). Naturally aged samples (Ga in orange, Pu in green)  $< 20$  years old are all 1.7 atom % Ga.

The heterogeneity was analyzed using the same wave separation method to give the results presented in Figures 10 and 13. These residuals or difference spectra were examined for spectral features that (1) are well fit by a Pu–Pu wave, (2) occur in identical or very similar form in multiple spectra, and (3) exhibit trends with [Ga] or age. Thus, in Figure 10, these difference spectra for the 2.4, 2.7, and 3.0 atom % Ga and the 3.3, 4.7, and 6.5 atom % Ga samples are overlaid to show that they divide into these two sets by virtue of, for the low [Ga] group, a common spectral feature at  $R = 3.8$  Å and, for the higher [Ga] group, one at  $R = 2.8$  Å. These features can be identified as simple Pu shells because, in addition to confirmation with curve fits, the real component has a minimum at the maximum of the modulus and relatively symmetric local maxima on each side. There are, of course, additional smaller spectral features that do not meet these three criteria. It must, however, be expected that, in the complicated process within the material that results in the nanophase separation, the sizes, shapes, and other parameters characterizing the domains of the second structure that will be dependent on [Ga] and the concentrations and types of other defects will produce a disordered fraction of the material that will not exhibit any trends if only because of the effects of destructive interference on EXAFS. This expected variability probably contributes to the fact that, although over a large number of samples from a variety of sources we have always found 3.3 atom % Ga to be the demarcation between material with and without the  $\sigma$  structure,<sup>8,93</sup> the recent report by a different group<sup>36</sup> found  $\sigma$  through a much higher [Ga] range. The focus must therefore be on the parts of the spectra that do comply with these criteria, particularly the reproducibility of the isolated spectral features. Although attempting to assign errors or uncertainties to these difference spectra would be futile, the reproducibility of the designated features, their correspondence with a Pu–Pu EXAFS wave, and their correlation with [Ga] demonstrate beyond cavil that there is significant specific action

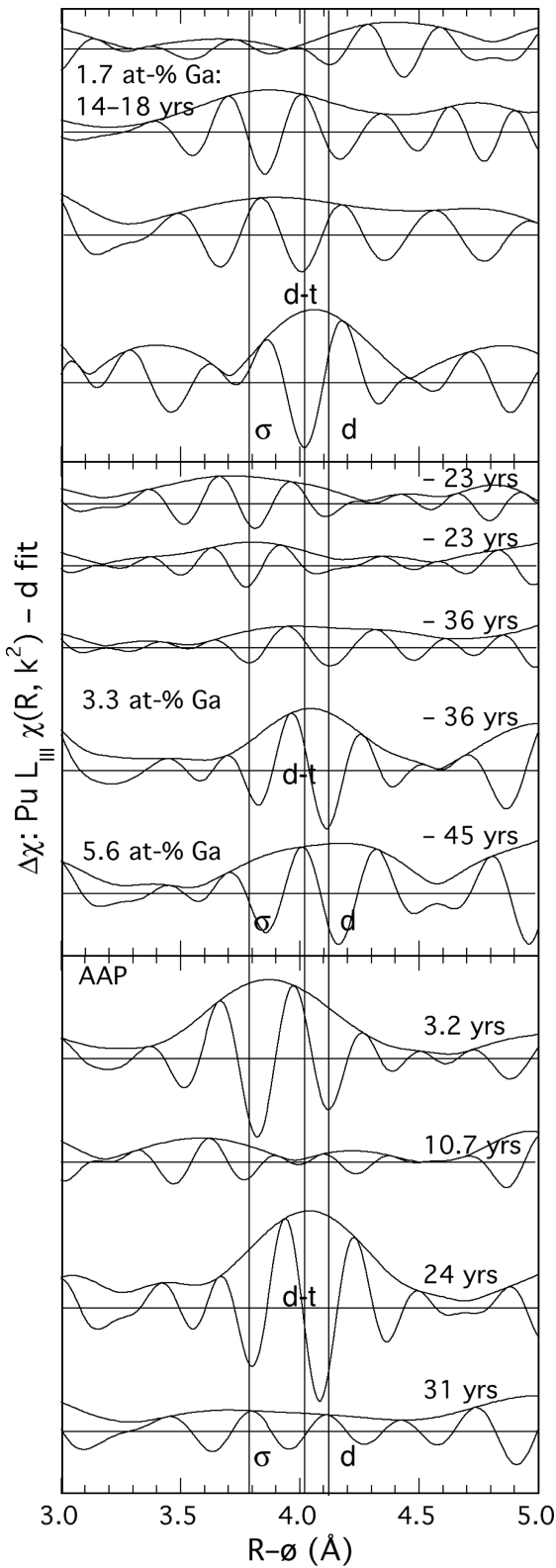


**Figure 13.** Same as Figure 10 but as a function of time in less ordered aged materials. The “ $\sigma$ ” line is the same as in Figure 10, aligned on the modulus peak and, for a simple Pu shell, the real component minimum so that the second spectrum from the top for the 1.7 atom % Ga may exhibit a somewhat displaced version of it and the 3.2 year old AAP sample definitely shows it. The “ $d$ ” and “ $d-t$ ” lines, also aligned with modulus peaks/real component minima, indicate the locations of spectral features in, respectively, materials with  $[Ga] \geq 3.3$  atom % that are  $\geq 36$  years old and materials with  $[Ga] \sim 1.7$  atom % that are

**Figure 13. continued**

$\leq 18$  years or 24 equivalent years that represent and can be fitted by simple Pu shells.

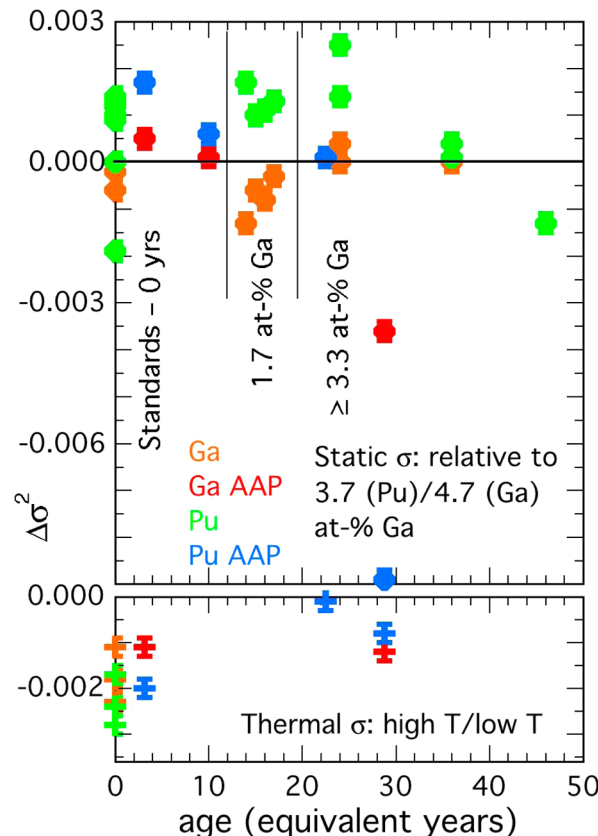


**Figure 14.** Same as Figure 8, but as a function of age. Blue symbols are the results for Pu in the AAP samples; red are for Ga in the same materials. As in Figure 8, positive values for the static component (the upper plot) indicate a smaller Debye-Waller factor than in the spectrum of the basis material.

in the local structure as a function of  $[Ga]$  beyond the periodic, crystallographic, fcc- $\delta$  portion of the material.

#### EXAFS Spectra of $\delta$ -Stabilized New $Pu_{1-x}Ga_x$ Samples.

Curve fitting and phase difference analyses demonstrate that the Pu–Pu distances for the first five shells of the  $\delta$  phase are within the error level ( $\pm 0.01$  for nn and up to  $\pm 0.04$  Å by the fifth shell near 7.3 Å) of  $\delta$  Pu for all the materials used here. Nor do any  $[Ga]$ -dependent changes in the Pu/Ga–Pu nn distances greater than  $\pm 0.015$  Å occur over this composition range for these samples, in contrast to those reported at very high Ga concentrations that were most likely caused by anharmonicity and/or neglecting discrete Ga neighbors in the analysis.<sup>87,88</sup> This is evaluated and discussed in more detail in a companion paper.<sup>93</sup> The Ga–Pu distances from these samples are also identical to those reported in the same references. The average interatomic distances are therefore of minimal interest with the important exception that the more distant ones do not contract with increasing  $[Ga]$  concomitant with the lattice parameter, indicating that the Vegard's law type behavior of  $\delta$  PuGa is not caused by a global change in the average structure.<sup>93</sup> It must instead originate in large displacements from the lattice for the atoms in proximity to Ga sites that overlap with displaced atoms from sites in proximity and the

resultant non-Gaussian pair distributions. The substantially reduced contribution to the EXAFS of these pairs of atoms that constitute the anharmonic portion of the distribution reduces their weight in the determination of the average distance for a particular shell so that the distance found by EXAFS will only be minimally or negligibly displaced from harmonic part that is centered on the lattice, as found here. An example of an anharmonic distribution resulting from small, asymmetric displacements of neighboring O atoms was found in  $\text{La}_x\text{Ca}_{1-x}\text{MnO}_3$ ,<sup>108</sup> and an especially good description of amplitude loss from an anharmonic portion of a neighbor distribution in  $\text{UO}_{2+x}$ .<sup>109</sup>

Notable behavior, however, does occur in the  $\delta$  Pu–Ga system, and inspection of the  $\chi(R)$  spectra of the new samples (Figures 5 and 6) is the starting point for its identification and characterization. [Ga]- and aging-dependent changes in the structure do affect the amplitudes of the EXAFS. Increasing [Ga] is expected to decrease the amplitude not only because of the mixing of the Pu–Ga and Pu–Pu waves as more Ga atoms occupy the neighbor shells but also because of the local disorder that the 4% smaller Ga atom induces in the positions of its neighboring atoms.<sup>86,88,90,110</sup> This disorder culminates when some Ga atoms must be at least second nn to each other in  $\text{Pu}_{0.935}\text{Ga}_{0.065}$ . Its spectrum at 35 K exhibits large shifts in the peak positions and shapes for  $R > 4 \text{ \AA}$ , with special attention given to the third nn contribution around  $R = 5.5 \text{ \AA}$  that is the second largest peak in the spectrum. An analogous modification of the  $R = 5.5 \text{ \AA}$  feature occurs for the material with the next highest [Ga],  $\text{Pu}_{0.953}\text{Ga}_{0.047}$ , at 90 K (Figure 6). This is of interest because it provides an observable demonstration of the martensitic equivalence of temperature and composition, whereby the temperature where structural phenomena coupled to the transformation occur will be higher in materials with stoichiometries closer to the transformation composition, which is around 1.0–1.5 atom % Ga for  $\delta$  Pu–Ga.<sup>16</sup>

The expected amplitude reduction with increasing [Ga] is observed in the Pu  $\chi(R)$ , but with a significant deviation. The modulus amplitudes of the principal nn Pu peak at  $R = 3.2 \text{ \AA}$  from lowest to highest [Ga] (Figures 5 and 6) are 0.34, 0.34, 0.35, 0.28, 0.34, 0.30, and 0.23 at 35 K and 0.21, 0.23, 0.24, 0.19, 0.21, 0.20, and 0.17 at 90 K, consistent overall with the expected nonlinear reduction of the average local order that will develop rapidly at some threshold value. The issue is what that value of [Ga] is, because the large decrease in the amplitude of this feature between the spectra of  $\text{Pu}_{0.963}\text{Ga}_{0.027}$  and  $\text{Pu}_{0.970}\text{Ga}_{0.030}$  is followed by a discontinuous jump in the spectrum from  $\text{Pu}_{0.963}\text{Ga}_{0.037}$  back or almost back to the high amplitudes of the low [Ga] samples, after which the amplitudes decrease monotonically. Insofar as this effect is reproduced at both temperatures it must be a characteristic of the sample, which in all other respects such as its diffraction pattern is normal, and not an experimental artifact. A concomitant effect in the Pu spectra is the loss of the large peak in the modulus around  $R = 3.8 \text{ \AA}$  that is observed for the 2.3, 2.7, and 3.0 atom % samples. This peak, its correlation with [Ga], its origin in a Pu shell that is not part of  $\delta$  Pu, the absence of any associated feature in the Ga EXAFS, and especially its loss or reduction to a minimal size around 3.3 atom % Ga and with age have been described previously.<sup>8,9,28</sup> We now find it here in the spectra of these ultrahigh purity materials with controlled homogenization times and temperatures that were not included in these prior reports. In contrast, for Ga the  $\text{Pu}_{0.983}\text{Ga}_{0.017}$  spectrum exhibits the lowest amplitude, after which the other spectra only display

small differences with no trend. These indications from the spectra of what effects result from changing [Ga], while useful in spotting patterns and anomalies, are nevertheless a poor guide to elucidating them in any meaningfully quantitative way because they reflect parameters in addition to the number of atoms like the Debye–Waller factor, leaving curve fits, ratioing, and similar methods as the only recourse. They can, however, now guide a more quantitative analysis.

**Numbers of nn  $\delta$  Atoms in New Pu–Ga Samples.** As discussed in the previous section, a key parameter is changes in the number of atoms in the nn  $\delta$  shell at  $3.28 \text{ \AA}$ , or, more accurately, the relative amount, since the disorder renders dubious assigning the nominal value of twelve even to the spectrum of  $\text{Pu}_{0.963}\text{Ga}_{0.037}$  that has the highest amplitude (and so was used as the basis for this calculation). Reductions in this number represent the shift or transfer of atoms from  $\delta$  Pu into other structures, especially when they are correlated with other spectral features such as the  $R = 3.8 \text{ \AA}$  peak; increases indicate the loss of such structures and the reversion of the atoms they contained back to  $\delta$  Pu. These more precise results obtained via the method described previously (Figure 7) corroborate the jump from 3.0 to 3.7 atom % Ga, which can now be seen to involve a 30% increase in the measured number of atoms in this shell concomitant with the loss of the peak at  $R = 3.8 \text{ \AA}$ , the 7% decrease for the highest [Ga] samples that could simply be the expected effects of the increased disorder and Pu–Pu/Ga wave mixing, and also find in addition a monotonic decrease of 12% on going from 1.7 to 3.0 atom % Ga. If the final three points belonging to the samples with the highest [Ga] represent the behavior of homogeneous  $\delta$  Pu–Ga, then even without the leap between the spectra from  $\text{Pu}_{0.970}\text{Ga}_{0.030}$  and  $\text{Pu}_{0.963}\text{Ga}_{0.037}$  the steeper slope of the four samples with the lowest [Ga] implies that the material is fundamentally different in this [Ga] range from the local structure perspective. The essential result, however, is that the EXAFS amplitude and, by implication, the fraction of Pu atoms involved in the  $\delta$  component of the material are always substantially greater above 3.3–3.7 wt % Ga and undergo an abrupt increase within that narrow range. Reductions in the amount of  $\delta$  Pu signify an increased number of Pu atoms in a different structure, that whose spectral signature is the peak at  $R = 3.8 \text{ \AA}$ .

The number of nn Pu around the Ga exhibits the opposite trend for the four samples measured at 35 and 90 K, a 22% increase in number between 1.7 and 4.7 atom % Ga and then a leveling off. This again corroborates the results from the spectra that indicate that the Pu and the Ga that substitutes for it in the lattice behave in almost antithetical fashion with changes in [Ga]. These changes in the fraction of the material occupied by crystallographic  $\delta$  Pu–Ga, the opposite behaviors exhibited by the Pu and the Ga, and their significance in identifying and characterizing the nanoscale heterogeneity are the crux of this report and will be evaluated in much greater detail following the presentation of the corroborating X-ray scattering and residual spectra.

**Debye–Waller Factors of nn  $\delta$  Atoms in New Pu–Ga Samples.** Possible changes in the element-specific static and thermal Debye–Waller factors—the widths of the Gaussian component of the Pu/Ga–Pu distribution—for the nn  $\delta$  shell are also of interest. The static component is useful in ascertaining the extent of harmonic disorder induced by the Ga atoms in the new samples and by the self-irradiation produced defects in aged samples.<sup>36</sup> The thermal component that is determined by measuring the temperature dependence

of the EXAFS  $\sigma$  is coupled to an important parameter for Pu, its elastic modulus.<sup>90,111</sup> Derived from the EXAFS, the Debye–Waller factor for a perfectly ordered shell in which all of the atom pairs of which it is composed have identical interatomic distances and bonds between them correspond to the vibrational amplitude of its atom pairs and thus samples the width<sup>112</sup> of the Pu–Pu/Ga–Pu potential well. The part examined in these measurements below the Debye temperature of around 100 K is the harmonic portion near its bottom. The potential is modified by internal stress in the material caused by defects and other inhomogeneities. Although just two temperature points are insufficient to quantify any changes and the relationship between this determination of the characteristics of the pair potential and the elastic moduli is too complicated to derive from this experiment, simply knowing if the average Pu–Pu and Ga–Pu potentials are or are not being affected by self-irradiation is critical in understanding Pu aging.

The differences in the Debye–Waller factors (Figure 8) of samples of different compositions and ages were obtained by logarithm-amplitude ratio analysis using the spectra of  $\text{Pu}_{0.963}\text{Ga}_{0.037}$  (for Pu) and  $\text{Pu}_{0.953}\text{Ga}_{0.047}$  (for Ga) as the basis for the static changes and a low temperature of 35 K and a higher one of 90 K for the thermal components. The static Pu–Pu Debye–Waller factor increases monotonically (in these figures a positive value corresponds to a lower Debye–Waller factor than that of the basis spectrum used in calculating this ratio) through  $[\text{Ga}] = 3.7$  atom % where (vide infra) the  $\sigma$  structure is initially lost. This trend is consistent with the heterogeneity being coupled to martensitic strain relaxation in the metastable [Ga] regime, with the local stress maximized when the material initially becomes homogeneous. The Debye–Waller factor subsequently rebounds, and then increases substantially for  $\text{Pu}_{0.935}\text{Ga}_{0.065}$  when all of the Pu atoms have on average a Ga in their second neighbor shell. Changes in the Ga–Pu environment are much smaller, reflecting its constancy and rigidity consistent with the static nature of the Ga local environment. The trend in the Pu–Pu Debye–Waller factors is consistent with earlier reports<sup>36</sup> if the gap between 4.3 and 7.0 atom % in [Ga] is large enough to have missed the decrease that we find after  $\text{Pu}_{0.963}\text{Ga}_{0.037}$  that would be associated with the decrease in disorder for this shell correlated with the loss of the  $\sigma$  structure superimposed on the monotonic increase expected from the Ga-induced disorder resulting from the smaller Ga–Pu bond length. Alternatively, this comparison is based on a single point, and the prior report does not find the increase between 3.0 and 3.7 atom % Ga that occurred in these and other samples. The trend in the Debye–Waller factors for the Ga–Pu bonds does match that from the other experiment. Although the Debye–Waller factor for the  $\sigma$  structure neighbor at 3.8 Å has not been analyzed—nor the number of atoms—it is clear (Figures 5 and 6) that the thermal component of its Debye–Waller factor is much smaller than that for the host  $\delta$  phase. Because its Pu–Pu distance is greater and the bond should be weaker, this implies that this bond is prestressed within the structure.

The thermal component of the Debye–Waller factor for the nn Pu–Pu bond at around 3.28 Å deviates from what might be expected in being almost constant across the entire range of [Ga]. Despite all of the indications of stress accumulation with increasing [Ga], there is no change in this vibrational amplitude of the Pu–Pu bond across the range of [Ga] until a possible, mild weakening at the highest Ga concentration. The  $\Delta\sigma$ 's obtained here are also similar to those previously reported for

1.9 and 3.3 atom % Ga samples,<sup>90,91</sup> a similarity reminiscent of the ultrasound measurements performed on this same sample suite.<sup>113–115</sup> The exception is the  $\text{Pu}_{0.973}\text{Ga}_{0.027}$  sample that was made from electrorefined instead of zone-refined Pu and was homogenized four times longer than the others. Its average Pu–Pu bond exhibits a much smaller change in the Debye–Waller factor, indicative of a narrower potential and demonstrating that process history can have a larger effect on the internal stresses and other parameters affecting the bond than composition by itself.<sup>84</sup> This finding contradicts the expectation that the width of the potential should be more strongly coupled to the nature of the bond than to longer range effects.<sup>116</sup> The variation in this temperature dependence for the Ga is much greater at the low [Ga] end, with the width of the nn Ga–Pu potential considerably more constricted in  $\text{Pu}_{0.983}\text{Ga}_{0.017}$  before increasing to its maximum at  $\text{Pu}_{0.970}\text{Ga}_{0.030}$  and subsequently narrowing somewhat at higher [Ga]. This behavior that we do not understand is the only characteristic of the Ga environment more sensitive to [Ga] than the Pu.

**Heterogeneity and the  $\sigma$  Structure.** The most unanticipated and unusual result from this set of Pu spectra begins with the spectral feature around  $R = 3.8$  Å for 2.3–3.0 atom % Ga that we have just shown transfers its weight to the nn  $\delta$  peak when it disappears at 3.7 atom % Ga and breaks the trend of monotonically reduced numbers of atoms in that shell with increasing [Ga] (Figures 5–7). A Pu shell at approximately 3.8 Å with around two atoms fits this part of the spectrum very well when it is present for  $[\text{Ga}] \leq 3.0$  atom %. The enhancement in the  $\delta$  ordering denoted by this jump in the number of nn  $\delta$  atoms even as [Ga] increases from 3.0 to 3.7 atom % can only occur if a non- $\delta$  fraction of the material present for  $[\text{Ga}] \leq 3.0$  atom % adopts the  $\delta$  structure within this [Ga] range. In addition, reiterating, the relative amplitude of this peak is larger at 298 K prior to cooling (Figure 6) where the large thermal motion dominates the amplitudes of  $\chi(R)$ , demonstrating that the atoms that give this non- $\delta$  feature have a smaller thermal Debye–Waller factor than those involved in the  $\delta$  structure.

This behavior therefore indicates the presence of a second Pu species in the form of domains of atoms embedded within the crystalline  $\delta$  lattice arranged in a structure different from  $\delta$ , the atoms of which join the host  $\delta$  Pu–Ga at this ~3.3 atom % Ga threshold. There are additional phenomena occurring at this [Ga] that indicate a coupling of the heterogeneity to properties on multiple length scales. Using the almost total relaxation of the Ga–Pu contraction at the third neighbor shell at 5.65 Å as the size of the local strain field around the Ga atoms,  $\text{Pu}_{0.967}\text{Ga}_{0.033}$  is where on average all of the Pu atoms are now within the strained volume surrounding the individual Ga atoms and the strain fields all come into contact with each other. This corroborates the idea that the atomic scale proximity of Ga suppresses the  $\sigma$  structure and favors the  $\delta$  one.<sup>67</sup> 3.3 atom % Ga is also where, macroscopically, the transition temperature of the martensitic transformation to  $\alpha'$  goes below 0 K so that  $\delta$  Pu–Ga is now stable instead of metastable. Thus, this second structure that we will call “ $\sigma$ ” most likely forms analogous to a spinodal in regions that are locally depleted in Ga. The basis of this assertion is the complete decoupling of the Ga and Pu EXAFS (Figures 5–7) in terms of (1) the opposite trends with [Ga] in the number of nn  $\delta$  atoms and (2) the complete absence of any signal in the

Ga EXAFS that disappears concomitantly with that at  $R = 3.8 \text{ \AA}$ .

The Pu in these Ga-depleted domains must rearrange into a structure inherent to the  $\alpha$  phase of Pu that is the stable form of pure Pu at these temperatures under the tension (negative pressure) exerted by the host  $\delta$  lattice and the constraints imposed by its interfaces with  $\delta$  Pu–Ga. Analogous behavior occurs in Fe, where the low density  $\alpha$  phase is produced when nanoscale domains or films are subjected to tensile stress when embedded in or on Cu with its larger lattice constant.<sup>10–13</sup> These domains might then be considered as the finest scale, spinodally based, martensitic texture, which according to martensite theory would therefore exist over the widest temperature range.

**X-ray Scattering Measurements and the  $\sigma$  Structure in Metastable Pu–Ga.** The existence and some information on the arrangement of atoms in this  $\sigma$  structure are corroborated by completely independent synchrotron X-ray scattering measurements on the same samples. A second, smaller amplitude  $Fm\bar{3}m$  type of diffraction pattern with a larger lattice constant is observed in the scattering data taken on some but not all of these samples (Figure 9), which we assign to the  $\sigma$  structure. This is consistent with the fact that a (quasi-)  $Fm\bar{3}m$  pattern with a lattice constant of 4.97–5.00  $\text{\AA}$  occurs frequently in the diffraction patterns from  $\delta$  Pu–Ga. This pattern has historically been assigned to PuO(C) deposits on the surface that coincidentally diffract in a very similar way. Although this interpretation is most likely correct for low energy laboratory X-ray sources with high surface sensitivity, the  $\sigma$  Pu we ascribe to this pattern is neither PuO(C) as might be suggested by the diffraction nor PuO<sub>2</sub> as might be suggested by the EXAFS and pdfs. Oxides and oxycarbides show a prominent nn O/C feature in the EXAFS that is absent here. (A recent, unpublished measurement of the XAFS of PuO(C) verifies that its spectrum is totally different from these.) In addition, contradicting this interpretation that assigns the smaller amplitude diffraction pattern and the  $R = 3.8 \text{ \AA}$  spectral feature to impurities are (1) the amount of oxycarbide would not be coupled to [Ga] as the  $R = 3.8 \text{ \AA}$  feature is; (2) at the 20% level we find it could be expected to include Ga atoms as well as Pu or else cause a significant reduction of the  $\delta$  Pu lattice constant if it caused Ga to diffuse into the uncorroded metal; (3) it would diminish with increasing X-ray penetration depth or be apparent in metallography and density measurements if it was part of the bulk and not limited to the surface; and (4) it would always give strong Bragg peaks when present in the local structure data. Conclusively, (5) indexing the  $\delta$  and  $\sigma$  diffraction patterns from a different set of Pu–Ga samples as reported in a separate manuscript<sup>93</sup> demonstrates that changes in the  $\delta$  lattice parameter with [Ga] are closely tracked in the  $\sigma$  structure. This could only occur if the minority structure was not present as inclusions within the first but necessitates that the two structures giving the diffraction patterns be intimately associated with each other in such a way, e.g., direct bonds, that the lattice constant of the minority one expands and contracts in concert with its majority host.

While the diffraction gives information on the periodic, long-range average structures, Fourier transforming the entire  $S(Q)$  function (actually  $F(Q)$ ) that includes the diffuse scattering that originates in disordered, aperiodic lattice distortions gives  $g(r)$ s, and implied pdfs, similar to those found by the Pu EXAFS.<sup>106</sup> Fascinatingly, these show that even when the diffraction displays only the  $\delta$  pattern,  $g(r)$  still contains peaks from the

$\sigma$  structure and so gives results identical within experimental error to those from EXAFS curve fits (Figure 9). The pdfs from the two independent methods are in exceptionally good agreement in terms of the number and locations of neighbor shells of atoms. Apart from errors in amplitudes from disorder and texture, the experimental pdfs are the sum of the calculated pdfs of  $\delta$  Pu with  $a = 4.64 \text{ \AA}$  and the fcc-like  $\sigma$  structure with  $a = 5.00 \text{ \AA}$  found by diffraction, except that it is modulated from fcc in that the expected shell near 3.5  $\text{\AA}$  is absent.<sup>93</sup> Assuming that the peak around 3.8  $\text{\AA}$  derives from the 3.5  $\text{\AA}$  distance required by the crystallographic constraints, then in order to retain this as an average distance it would need to be mirrored by one near 3.2  $\text{\AA}$  that falls within the envelope of the nn  $\delta$  shell at 3.28  $\text{\AA}$  in both  $g(r)$  and  $\chi(R)$ . The effect of this modulation diminishes rapidly with distance so that the separations of more distant shells are less than their width and they occur as only a single, somewhat broadened peak.

This is a remarkable result in that it clearly shows how the scattering data contain the information defining the (identical) ordered  $\sigma$  structure both when the  $\sigma$  domains are sufficiently large and correlated to diffract as well as when they are so small and aperiodically arranged that they do not. The non- $\delta$  atomic density peaks indicate that, consistent with the Bragg peaks when they occur, the up to 20% of the atoms in  $\sigma$  domains order as another quasi-fcc modulated by the splitting of the first shell that should be and whose average is still at 3.5  $\text{\AA}$ .

The  $\sigma$  structure does not correspond with any of the known Pu phases, consistent with our interpretation of pure Pu at  $\leq 300 \text{ K}$  under tension. The apparent splitting of the 3.5  $\text{\AA}$  Pu–Pu distance indicates that  $\sigma$  Pu has a modulated structure in which the cubic unit cell is multiplied<sup>82</sup> and the original cubes alternately expanded and contracted,<sup>93</sup> retaining the cubic structure on average with only minimal effects on the overall diffraction pattern<sup>8</sup> in which superlattice peaks would be obscured because of the domination of  $S(Q)$  by the majority  $\delta$  Pu–Ga phase. The  $\delta$  density is easily conserved in this expanded structure by adding interstitials within the large cubes, where they give short bond lengths comparable to those found in  $\alpha$  Pu and (vide infra) the “ $\sigma$ ” variant of this structure we postulate for the  $\text{Pu}_{0.983}\text{Ga}_{0.017}$  sample in this set. Intriguingly, this modulation not only gives the  $\delta$  Pu bond length but also splits the nn shell so that the ratio of its short and long distances is that of a bcc structure, implying that the modulation occurs along a soft Bain path<sup>82,113,114</sup> that may involve a second,  $\epsilon$  Pu-like electronic structure.<sup>117</sup> The phonon dispersion curves do in fact show soft deformation paths, both this tetragonal distortion and a [111] shear, that provide deformation mechanisms by which new structures could easily form.<sup>80,83,85</sup>

The interplay of local elastic forces with the  $\delta$ -stabilization mechanism and the resulting heterogeneity are apparent in that (1) the more homogenized sample that should have better defined  $\sigma$ – $\delta$  interfaces gives a larger  $\sigma$  peak (cf. Figure 5 and 6) and (2) this sample of ultrapure  $\text{Pu}_{0.983}\text{Ga}_{0.017}$  is the only one we have measured in this concentration range whose EXAFS does not show the  $\sigma$  signature.<sup>8,93</sup> However, insofar as the amplitude of its Ga EXAFS is reduced (Figures 5 and 6), this “ $\sigma$ -less” 1.7 atom % Ga sample must possess at least one other type of Ga environment in addition to the  $\delta$  one of the host lattice. In the Pu spectrum, instead of a peak near  $R = 3.8 \text{ \AA}$ , a prominent feature occurs around  $R = 2.5$ – $2.6 \text{ \AA}$  on the low  $R$  side of the main peak of the  $\text{Pu}_{0.983}\text{Ga}_{0.017}$  Pu  $\chi(R)$  spectrum at all temperatures (Figures 5 and 6). This suggests that the local

ordering within the  $\sigma$  domains is altered when they are large at low [Ga] and so contain Ga and possibly other impurities. It is thus likely that what we will call the “ $\sigma'$ ” variant with its putatively larger Ga-depleted, non- $\delta$  domains also differs from  $\sigma$  in incorporating some of the Ga atoms, albeit in disordered environments invisible to EXAFS. Local ordering around the longer bonds in the cubic lattice therefore gives the  $\sigma$  structure in the smaller Ga-depleted domain. In the larger domains that occur at lower [Ga] where the energy associated with the structure is higher and that with the  $\delta$  interface is less, ordering around the shorter, interstitial-centered distances may be the origin of the more  $\alpha$ -like “ $\sigma'$ ” behavior observed in this 1.7 atom % Ga sample.

**Difference EXAFS and the  $\sigma$  Structure in Metastable Pu–Ga.** In the EXAFS, the identification and characterization of the  $\sigma$  structure and, *vide infra*, additional ordered non- $\delta$  substructures are better performed when, as described above, the contributions of the  $\delta$  structure are removed by curve fitting the data with only the  $\delta$  shells and then subtracting them out, isolating the non- $\delta$  atoms for separate evaluation (Figure 10). By overlaying spectra that contain a shared feature so that the shape and location of its modulus and real component can be directly compared against the others, these difference spectra reveal the common [Ga]-dependent spectral (and by implication structural) attributes observed in the full spectra and coupled to their behavior. The isolation of these features also allows them to be inspected for the distinctive pattern of the Pu–Pu EXAFS waves used to fit them so as to confirm that they correspond (or not) with simple, Pu shells not belonging to the  $\delta$  structure. Using this method, the modulus peak at  $R = 3.7\text{--}3.8 \text{ \AA}$  in the full Pu spectra of the 2.3–3.0 atom % Ga samples that has already been associated with a non- $\delta$  component that is closely coupled to diminished amplitude of the nn  $\delta$  Pu is seen to be a large, clean, well behaved independent peak in these residual difference spectra that only occurs over that [Ga] range. Overlaying the residuals from these three samples shows that these spectral features display an identical pattern in the real component and very similar moduli that signify an ordered Pu shell (for this data range the modulus peak coincides with a minimum in the real component) near  $R = 3.8 \text{ \AA}$ . These difference spectra thus corroborate the curve-fit results that find a Pu shell at  $3.77\text{--}3.81 \text{ \AA}$ . This feature is notably absent from the difference spectra of the  $\text{Pu}_{0.983}\text{Ga}_{0.017}$  and  $[\text{Ga}] > 3.4$  atom % samples, showing that if, e.g., a fraction of a Pu atom near this distance were to improve the curve fit by removing noise that distorts the baseline in this region, it would be an artifact of the fit.

The  $\sigma'$  structure described for  $\text{Pu}_{0.983}\text{Ga}_{0.017}$  gives a modulus peak near  $R = 2.6 \text{ \AA}$  coincident with a node in the real component instead of a minimum, demonstrating that it is not a simple Pu shell. This spectral feature, which was present prior to cooling (Figure 6) in a sample that showed no trace of the  $\alpha$  Pu diffraction pattern, is identical to the one from the 2.5–2.7 Å Pu–Pu pairs in  $\alpha$  Pu.<sup>118</sup> As already suggested, it therefore signifies a very similar complicated Pu distribution around this short distance. This range of shorter Pu–Pu distances in  $\sigma'$  are ordered in a very  $\alpha$ -like way that would be consistent with the larger Ga-depleted domains expected to occur in this sample with minimal impurities and the lowest [Ga].

The surprise in this analysis is the observation of the “ $\delta$ ” simple Pu-type feature at  $R = 2.8 \text{ \AA}$  in the spectra of the samples with  $[\text{Ga}] > 3.4$  atom %. These, and especially  $\text{Pu}_{0.963}\text{Ga}_{0.037}$ , could have been expected to be homogeneous  $\delta$ ,

but instead they apparently all exhibit a common, Pu-based lattice distortion at a short,  $\sim 2.8\text{--}2.9 \text{ \AA}$  distance even across this relatively large [Ga] range. Our best guess at this time would be that it originates in response to the overlap of the local strain fields around the Ga atoms, an effect that would therefore begin immediately after the Ga distributes through the lattice in a way that eliminates the Ga-depleted domains where the  $\sigma$  structure forms so that the preference for Ga–Ga distances  $\geq 5 \text{ \AA}$  that gives the quasi-metallic can no longer be adhered to. This finding may also, however, corroborate the proposal that the electronic structure and bonding in  $\delta$  Pu–Ga are anisotropic.<sup>67</sup>

This compilation does not necessarily encompass a complete list of non- $\delta$  lattice distortions. The possibility of additional features occurs with, e.g., the peaks at  $R = 4.7 \text{ \AA}$  for  $2.3 \leq [\text{Ga}] \leq 3.0$  atom % and at  $R = 3.5 \text{ \AA}$  for  $3.7 \text{ atom \%} \leq [\text{Ga}]$ . These, however, are lower in amplitude than the irreproducible regions of the overlaid spectra and therefore possibly near the overall noise level. Moreover, the goal of this exercise is not to develop an exhaustive list of non- $\delta$  nn shells but to simply identify the most prominent ones that could be coupled to [Ga] and additional structural and other properties.

### The Composition Independence of the Ga EXAFS and Ga Organization.

Like the  $\delta$  Pu, component, the curve-fit derived distances between the smaller Ga and the larger Pu atoms in these samples are very similar to those previously reported<sup>36,86–90</sup> and do not vary with [Ga] (and will be reported in detail elsewhere<sup>93</sup>). However, in contrast to the [Ga]-dependent changes in the Pu EXAFS, the highly ordered Ga EXAFS (Figures 5 and 6) exhibit only minimal differences for  $[\text{Ga}] > 1.7$  atom % to very high  $R^{88,89,92}$  and even the  $\text{Pu}_{0.983}\text{Ga}_{0.017}$  spectrum is identical to the others except for its diminished amplitude. One contribution to this preservation of the Ga environment over almost a factor of 4 in [Ga] is that, since the average Pu–Pu and Ga–Pu distances of the  $\text{Pu}_{12}\text{Ga}$  cuboctahedron are equal, these Pu–Pu bonds must be compressed to a distance below that of the minimum in their  $\delta$  pair potential whereas the Ga–Pu bonds are longer than the minimum of the Ga–Pu potential. This prestressing of the Ga environment explains its stiffness *vis-à-vis* the Pu–Pu bonds,<sup>48,90</sup> although anisotropy in the Pu–Pu bonding vs spherical symmetry in the Ga electronic structure<sup>67</sup> would also contribute. It is also significant in the relationship of the microscopic mechanism of the substitution of the Pu by the smaller Ga atoms to the bulk lattice reduction, i.e., Vegard’s law.<sup>86,88</sup> The Ga–third nn Pu shell distance is only around 0.01–0.03 Å shorter than the Pu–Pu one. This relaxation from the 0.12 Å contraction for the first nn shell to almost zero sets the diameter of the local strain field around the Ga at this third shell distance of around 11–12 Å. This contraction is significantly less than the 0.045 Å calculated from Vegard’s law for 5.75 Å and the difference between the nn Ga–Pu and Pu–Pu distances found by EXAFS. The accelerated relaxation of the strain around the Ga indicates that there must be contributions to the bulk lattice contraction in addition to the simple displacement of the Ga neighbors.<sup>93</sup> The important one most likely occurs when a pair of Ga atoms is within 11 Å of each other so that their local strain fields overlap. The stiffness of their local environments would cause the Ga atoms to be displaced from their lattice sites toward each other so that their overlapping Pu neighbors remain at the same distance from both, pulling sets of adjacent Pu atoms with their softer potentials along the displacement vector. The bulk contraction

would therefore result when these strain “stripes” overlap to form extended networks, with the coupling between composition and size caused by the enhancement in the extent of these networks as [Ga] increases. We have performed (but not included here) calculations that show the nonintuitive result that the highly nonlinear dependence of the number of these long-range Ga–Ga interactions on [Ga] in combination with this percolation-type mechanism actually gives linear, Vegard’s law type behavior over the stability range of  $\delta$  Pu–Ga.

Although this prestressing of the Ga sites is necessary to duplicate the behavior of the Ga EXAFS, it is nevertheless also insufficient. Extensive MD-type modeling (also not included here) shows that eliminating Ga-centered disorder so as to match the [Ga] independence displayed by these experimental data requires harmonic Ga–Pu potentials >1500 times as deep as the Pu–Pu ones outside the Ga strain field, obviating relative bond strength and width as the sole means for explaining these spectra. Composition independence for the Ga EXAFS is, however, readily attained by eliminating a random placement of Ga atoms in favor of “organizing” them relative to each other in the crystal by augmenting the probability for Ga atoms to be at certain distances and angles relative to each other. An intriguing corollary is that angular dependence for Ga triplets and higher combinations would lower the symmetry from cubic to tetrahedral and orthorhombic, an effect that would be obscured if differently oriented domains remained coherent.<sup>6</sup> The effect is less than the strict ordering in an intermetallic, which in any event could only occur for a few precise stoichiometries, but does give a “quasi-intermetallic” type of structure in which the ordering is a preference rather than a rule, but strong enough to result in Ga clustering and the  $\delta$ – $\sigma$  nanoscale heterogeneity. Using the ca. 11.5 Å diameter of the Ga local strain field, 3.3–3.5 atom % Ga as the point around where the  $\sigma$  structure is lost and the material becomes homogeneous  $\delta$  and the composition where the Ga EXAFS are ultimately disordered by increasing [Ga],<sup>87,88</sup> the Pu:Ga ratio for this organized structure would be around 25–35:1. This collective behavior that clusters the Ga atoms has the additional effect of increasing the fraction and domain sizes of Ga-depleted material in the crystal where  $\sigma$  Pu forms beyond what would occur with a random distribution as well as giving the  $\delta$  Pu–Ga fraction a consistent, homogeneous structure. In terms of the prior controversy of whether  $\delta$  Pu–Ga is more or less stable than  $\alpha$  Pu + Pu<sub>3</sub>Ga,<sup>39</sup> this result suggests that a quasi-intermetallic with a high Pu:Ga ratio is another competing phase. Or, in light of recent LDA-DMFT calculations<sup>69,74</sup> and experiments demonstrating the proposed multiconfiguration electronic structure,<sup>75</sup> Pu<sub>30</sub>Ga could simply represent a different admixture of quantum states than these others. Thus, the complete description of the structure of  $\delta$ -stabilized Pu–Ga must include the formation of separate  $\delta$  Pu<sub>30</sub>Ga and  $\sigma$  Pu domains with  $\sigma$  Pu disappearing as Pu<sub>30</sub>Ga fills and ultimately saturates the crystal.

A quasi-intermetallic could also help explain the additional, “ $\delta$ ” lattice distortion (Figure 10) for the [Ga] > 3.4 atom % samples. This does appear as a simple Pu shell so that, once revealed by the  $\delta$ -subtraction method, its inclusion does improve curve fits by giving a small Pu shell around 2.85 Å. It is plausible that this peak is part of the postulated Pu<sub>30</sub>Ga since its amplitude does not track [Ga]. Although it has been assumed that the substitution of Pu by Ga is simple so that the first three peaks of the Ga  $\chi(R)$  spectra are assigned to the first three neighbor shells of a symmetrically contracted fcc site, the Ga EXAFS—and by implication its local structure—differs in

certain respects from both that of the Pu and simulations, such as its long-range features beyond the third shell. Furthermore, since the Ga spectra are invariant over this composition range (Figures 5–7), Ga-centered lattice distortions cannot be identified vis-à-vis differences in the calculated amplitudes and phase shifts by tracking changes with [Ga] so that the residuals from the Ga EXAFS may or may not indicate further complications in the structure. A lowering from fcc symmetry such as has been found in NMR<sup>119</sup> could be obscured in the putatively quasi-cubic Ga EXAFS. Alternatively, since the Ga environments remain highly conserved even beyond saturation of the crystal with Pu<sub>30</sub>Ga up to very high [Ga], the distortions might be the response of Pu<sub>30</sub>Ga to the incorporation of extra Ga atoms.

**Aging Effects and Nanoscale Heterogeneity in  $\delta$  Pu–Ga.** This heterogeneity resulting from the tendency of the Ga (and other) impurities and defects to aggregate and organize and for the Ga-depleted (and other local composition-based) domains to rearrange into structures different from the  $\delta$  host is also critical in understanding the effects of the self-irradiation.<sup>36</sup> The  $\alpha$  decay of the Pu is an important effect in that it is estimated to displace every atom from its original lattice site once every ten years on average. The overwhelming majority of the atoms disrupted by the U recoil nucleus—and it has even been suggested that the material melts along its path—return to lattice sites so that the crystallinity is only lost slowly over decades or longer (Figure 11). Some, however, do not, and their fate is critical in developing a predictive model for the effects of radiation damage. Representative EXAFS spectra show a variety of effects (Figure 11). The naturally aged Ga spectra show minimal or negligible indications of changes in the structure—cf. the spectrum of 36 year old Pu<sub>0.9967</sub>Ga<sub>0.033</sub>—other than a general loss of amplitude that can be attributed to a parallel loss of order as the material slowly becomes more amorphous. In naturally aged Pu samples, as will be shown, the effects of self-irradiation on the local structure are convoluted with the composition dependence just discussed and require a more detailed analysis. In contrast, both the Ga and the Pu EXAFS of the AAP samples show relatively fast losses of amplitude that are not always even throughout the  $\chi(R)$  spectra and suggest that such effects may exhibit some dependence on the self-irradiation rate. Exemplified by the modulus peak at  $R = 4.0$  Å in the Pu spectrum from the naturally aged 24 year old sample, these non- $\delta$  spectral features must represent the growth and loss of ordered structures like the  $\sigma$  one (cf. Figures 12 and 13) and a second channel by which radiation-induced defects are stabilized off of  $\delta$  lattice sites in addition to the much less organized formation of randomly distributed point defects. The stabilization of radiation-induced defects is critical since the sensitivity of EXAFS is such that a spectral feature will not appear unless the shell it represents contains on the order of 10% of the atoms in that distance range, a number that is 1–2 orders of magnitude larger than typical for radiation damage. We have found such stabilization at internal interfaces, such as those that would occur between the  $\delta$  and  $\sigma$  or differently oriented tetragonal structures.<sup>6</sup> Stabilization at particular locations will result in locally high defect concentrations that could lead to additional decreases in energy via cooperative rearrangements into novel structures and, *vide infra*, nanoscale heterogeneity redux. Although somewhat obscured by the effects of texture, X-ray diffraction patterns as samples age (Figure 11) do not show any significant Q-dependent transfer of scattering weight from the Bragg peaks into the broad diffuse

scattering background, supporting the contention that the radiation damage is forming ordered structures that diffract poorly because, e.g., they are below the diffraction limit size and may be coherent with the host  $\delta$  lattice.

The appearance of novel features in the Pu (but not the Ga) EXAFS spectra concomitant with the loss of amplitude from the  $\delta$  structure supports the contention that aging may produce effects analogous to those observed with [Ga]. Extensive modeling of the EXAFS of a number of Pu–Pu distributions verified that the observed reductions in amplitude are not just strain-induced anharmonic modifications of the  $\delta$  shells but most likely reflect heterogeneity similar to that posed by the  $\sigma$  structure in terms of shifts of a fraction of the atoms from the nn  $\delta$  shell to specific new positions that result in the formation of ordered non- $\delta$  structures in the crystal. It is therefore useful to analyze and interpret the spectra in an identical way to those of the new materials, beginning with measured changes in the numbers of atoms residing in the ordered  $\delta$  component of the material. This is also a useful parameter for evaluating microscopic radiation damage that has accumulated in aged samples because it is a measure of the conventional radiation-induced disorder, e.g., Frenkel pair formation, etc. Within this interpretation, ordinate values  $>100\%$  most likely result from the formation of new Pu–Pu pairs at the 3.28 Å  $\delta$  bond length because of the transformation of non- $\delta$  types of structures with different near neighbor distances. The relative numbers of atoms in the nn  $\delta$  shell at 3.28 Å Pu extracted from the  $\chi(k)$  spectra of the aged 1.7 and 3.3 (and the one 5.6) atom % Ga samples show (Figure 12) substantial scatter (especially for the Pu) and therefore by themselves offer little or no insight into the damage mechanisms. In fact, the absence of the expected monotonic decrease consistent with an increase in the concentration of radiation-induced, non-interacting point defects would, within the framework of conventional models, suggest that all that is being observed is noise. The explanation for this result as a real phenomenon and its significance with regard to radiation effects is, however, found when changes in the nn numbers of atoms are correlated with the non- $\delta$  spectral features found in the residual spectra that would account for the reduction in the fraction of  $\delta$  material, identified by the same method used for the new samples as the residuals in difference spectra after fitting the EXAFS with the  $\delta$  neighbor shells (Figure 13).

### Collective and Element Specific Behavior and Aging

**Mechanisms.** Although the features in the residual difference spectra (data with the  $\delta$  shells removed) of the aged samples (Figure 13) are somewhat more obscured and variable than those in the same spectra from the models (Figure 10)—a not unexpected effect insofar as they are more difficult to prepare and should possess more disorder—consistent features corroborated by curve fits are found with this technique. The zeroes and minima in the real component are a more consistent guide than modulus peaks. In addition to the 3.8 Å Pu shell diagnostic for the  $\sigma$  structure in some of the younger samples, a new, non- $\delta$ , aging-associated, Pu shell (labeled “d” in Figure 13) occurs that is the  $R \sim 4.12$  Å modulus peak in the full Pu  $\chi(R)$  of 36 year old  $\text{Pu}_{0.996}\text{Ga}_{0.033}$ . The position of this feature shifts to slightly higher  $R$  with increasing [Ga], although in this sample set age and [Ga] are correlated. While the residual spectrum of the  $<20$  year old 1.7 atom % Ga samples at the top of Figure 13 shows nothing, the second from the top exhibits the  $\sigma$  (at a slightly higher  $R = 4.1$  Å) and possibly  $\sigma'$  (not shown) features, and the two lower ones without  $\sigma$  show the

real component/modulus “d–t” combination for a simple Pu shell (Pu–Pu distance = 4.0–4.1 Å) just above  $R = 4.0$  Å that must have formed as a result of initial aging processes. Naturally aged samples with [Ga]  $> 3.4$  atom % display modest amounts of the  $\sigma$  signature when  $<30$  years old, possibly  $\sigma'$  for one sample, and no  $\delta$ . Spectra from [Ga]  $> 3.4$  atom %  $>30$  year old samples, however, not only contain possible  $\delta$  features and no sign of  $\sigma$  but also show the “d” spectral feature of a Pu shell at  $R = 4.1$ –4.2 Å (Pu–Pu distance = 4.06–4.10 Å). Unlike the  $\sigma$  structure, diffraction peaks from the structures containing this shell of atoms were never observed and pdfs were never measured so that this feature is simply a diagnostic showing that the self-irradiation results in an ordered lattice distortion involving a significant fraction of the Pu atoms in the sample. In addition, radiation-induced atom displacements in materials with  $>3.3$  atom % Ga appear to accumulate more slowly and form a slightly different locally ordered structure than in those with lower [Ga], suggesting that high [Ga] materials may be more resistant to these microscopic self-irradiation effects.

To reiterate, the absence of a trend in the numbers of atoms in the nn  $\delta$  shell is thus comprehensible via their now demonstrated correlation with the ordered lattice distortions and heterogeneity: lower numbers of nn Pu atoms correlate with the observation of ordered non- $\delta$  structures and higher nn Pu numbers occur when only the  $\delta$  structure is present. In addition to the formation and loss of the [Ga]-dependent  $\sigma$  structure, changes in the number of atoms in the Pu nn shell also track the various time-dependent arrangements of atoms signified by the d and d–t spectral features. The presence of  $\sigma/\sigma'$  structures reduces the number of atoms in this shell at 3.28 Å, although the  $\delta$  structure apparently does not. This would occur if the  $\sigma/\sigma'$  structures possess shells of atoms whose distances differ from the nn  $\delta$  one by 0.05–0.25 Å, resulting in destructive interference between the EXAFS waves. Thus, the lowest  $\delta$  nn amplitudes are found for both new and aged samples that display  $\delta-\sigma/\sigma'$  heterogeneity. One of the first effects of age is the loss of  $\sigma/\sigma'$ ,<sup>8,27,28</sup> which increases the nn  $\delta$  shell amplitude and gives a spectrum resembling homogeneous  $\delta$  Pu–Ga with  $>3.3$  atom % Ga. Such an effect could result from a dispersing of the Ga atoms of  $\text{Pu}_{30}\text{Ga}$  along the track of the U recoil nucleus to give a more even nanoscale Ga distribution that eliminates the Ga-depleted domains. Alternatively, if the defects emulate Ga in stabilizing the  $\delta$  structure, their formation in the Ga-depleted domains would convert these regions from  $\sigma$  to  $\delta$ .<sup>120</sup> As more defects accumulate, the material passes through this transitory homogeneous  $\delta$ -like state, rapidly and with more variability for  $\text{Pu}_{0.983}\text{Ga}_{0.017}$ , more slowly and consistently for  $\delta$  Pu–Ga alloys with higher [Ga]. However, at longer times, the defects appear to be stabilized by forming yet a third kind of ordered structure that is derived from and thus again lowers the number of nn Pu atoms from the  $\delta$  structure and whose structure varies somewhat between higher and lower [Ga].

The AAP material follows the same process (Figure 13). Its initial  $\delta/\sigma$  state has a low nn  $\delta$  shell relative amplitude of only 88 of the standard (relative to standard = 100) that increases to 111 (Figure 12) when  $\sigma$  is first lost (Figure 13) at 10.7 years. It diminishes again at 22 years time to 78 when a large amount of damage has accumulated and heterogeneity again occurs as the “d–t” feature centered around  $R = 4.02$  Å that is well fit with a Pu shell in some of the spectra from materials with lower [Ga] that have aged for  $<20$  years. Some of these spectra may also exhibit the  $\sigma'$  feature, which if this assignment is correct would

indicate a greater susceptibility to cooling-induced transformation in aged materials. Consistent with the  $\chi(R)$  (Figure 11), the only significant difference between the AAP and naturally aged material is that the enhanced rate of radioactive decay may have accelerated the rate at which the defect concentration increases so that for the same number of decays the latter is higher for the AAP material than for naturally aged, i.e., the rate of aging in terms of the number of defects in the material is coupled to the rate of self-irradiation. This is consistent with the idea presented herein that the defects interact to form stable structures since the higher steady state concentration of radiation-induced defects resulting from a higher specific activity would increase the probability of two or more defects overlapping with and stabilizing each other before they can relax back to the original structure. In the final measurement at 29 years, the AAP  $\text{Pu}_{0.983}\text{Ga}_{0.017}$  no longer appears to sustain any ordered defects as its overall appearance is more amorphous and the amplitude of the nn rises again, although only to 89. Caution must be exercised, however, in extrapolating this assessment. Unlike, e.g., Pu-containing oxides subjected to accelerated self-irradiation,<sup>121</sup> this material still possesses substantial long-range order in its diffraction pattern (Figure 11). Some portions must remain relatively unaffected, or else even as atoms are displaced from their lattice points the lattice itself and its average long-range order are conserved. This is consistent with the finding that  $\delta$  Pu–Ga is much more radiation resistant than other metallic Pu compounds.<sup>36</sup>

The behavior of the Ga site with aging recapitulates that found for composition: although the overall spectral amplitude can be diminished by the heterogeneity apparent in the Pu—especially by the presence of  $\sigma'$ —there are only small shifts in the positions and shapes of the smaller features of the spectra of materials with different histories and it is difficult to find spectral signatures associated with lattice distortions (Figure 11). As would be expected of a stable, quasi-intermetallic type of structure dictated by Ga interactions, the Ga environment is much more conserved throughout synthesis, fabrication, and aging than the Pu one and when there are Ga atoms in structures other than  $\delta$  they are highly disordered. That the Ga environment is only minimally or negligibly affected by aging implies that the aging-induced defects, whether isolated or as novel ordered structures, almost exclusively involve Pu sites and are thus concentrated in Ga-depleted domains in the crystal that must therefore reform if they are lost at some point in the aging process. The aggregation of age-induced defects into ordered structures could stabilize these domains so that the reduction in recombination rates would account for their quantity, tens of percents. Like the Pu, however, this trend is eventually overwhelmed at longer times and the Ga environment also loses long-range order concomitant with the Pu. Remarkably, this aging process in  $\delta$  Pu–Ga is the opposite to that in  $\alpha$  Pu, whose local structure displayed only negligible differences from the crystal structure in aged samples.<sup>118</sup>

**Debye–Waller Factors of the Nn  $\delta$  Pu Shell in Aged Materials.** As with the new samples, differential Debye–Waller factors (Figure 14) for aged materials were obtained by logarithm-ratio analysis using the  $\text{Pu}_{0.963}\text{Ga}_{0.037}$  (for Pu) and  $\text{Pu}_{0.953}\text{Ga}_{0.047}$  (for Ga) spectra for the static changes and a low temperature of 25–40 K and a higher one of 85–95 K for the thermal behavior. The static Debye–Waller factor for the nn  $\delta$  Pu–Pu shell at 3.28 Å has already been shown to be mostly conserved in the new samples, except that it is larger for  $\text{Pu}_{0.963}\text{Ga}_{0.037}$  after the  $\sigma$  structure is initially lost and then

increases substantially for  $\text{Pu}_{0.935}\text{Ga}_{0.065}$  when all of the Pu atoms have on average a Ga in their second neighbor shell. Extending this evaluation to aged materials, for most samples smaller nn  $\delta$  Pu–Pu Debye–Waller factors are correlated with  $\sigma/\sigma'$ , d, and d–t heterogeneity in aged  $\text{Pu}_{0.983}\text{Ga}_{0.017}$ , consistent with the distortions forming to relieve defect-induced lattice strain. The existence of competing structures in  $\delta$  Pu–Ga is therefore an important aspect of its response to stress, including aging-induced defects. This same trend is also displayed by the AAP samples, with a dramatic increase in the longest time when the breakdown of order beyond the nn shell without concomitant formation of preferred noncrystallographic distances could be expected to substantially broaden the distribution around the Pu–Pu bond. The Ga–Pu static Debye–Waller factors are, like the EXAFS spectra from which they are derived, much less variable. However, similar to the Pu, the final AAP measurement shows a very large increase coincident with the severe loss of order in the structure that, as shown in Figure 12, has affected even the Ga environments.

The thermal components of the Debye–Waller factors for the nn  $\delta$  Pu–Pu bond in these aged materials are substantially smaller than the value of −0.0024 around which the values from the new samples were clustered. Since this parameter is associated with its width and the slopes of the pair potential near the bottom of the well, lower numbers imply that this potential becomes narrower and steeper with age, which could be expected as the accumulation of defects disrupts the local order and stresses the bonds. This result might be taken to suggest that  $\delta$  Pu–Ga would require more energy to compress as it ages. However, insofar as this disruption with aging involves the formation of defects that have softer potentials, it cannot be extrapolated to suggest that the elastic moduli would increase. In fact, the material as a whole will soften with age if the defects are randomly distributed soft ones. Since these experiments show that that does not appear to be the case in that the defects are stabilized in clusters in Ga-depleted regions that exhibit specific lattice distortions to form novel structures, the response of its elastic moduli to aging is difficult to predict. The observed narrowing of the potentials would nevertheless be useful in developing and evaluating microscopic models. The interpretation of the thermal component of the nn  $\delta$  Ga–Pu pair is more problematic because it exhibited some [Ga] dependence in the spectra of the new samples. Using the lowest value of around  $-0.0011 \text{ \AA}^2$  that was found for the same [Ga] as in the AAP samples, aging produces virtually no change in the nn  $\delta$  Ga–Pu potential even at the longest time where the static Debye–Waller factor of this pair had greatly increased. The Ga–Pu bonds are generally stiffer than the Pu–Pu, with that in  $\text{Pu}_{0.93}\text{Ga}_{0.017}$  being especially strong despite its static component being broader than in the spectra of the other new samples, suggesting that this site is stressed. The Ga–Pu bond in the previously measured  $\text{Pu}_{0.967}\text{Ga}_{0.033}$  sample<sup>90</sup> had a  $\Delta\sigma^2$  very close to that of the  $\text{Pu}_{0.983}\text{Ga}_{0.017}$  basis material.

**The Energy Landscape of Complex Crystalline Solids.** Supplemented by the X-ray pdf and diffraction, these EXAFS measurements clearly give a radically different description of the structure and behavior  $\delta$  Pu–Ga than any previously offered in the literature. But they also offer an equally clear basis for this finding, unequivocally demonstrating that despite the fact that Ga substitutes for Pu and is found on the lattice sites of  $\delta$  Pu–Ga crystal its behavior in the lattice is at variance with that of the Pu not only in new materials but also in the aging process. This retention of the original elemental identities of

the constituent Ga and Pu atoms, despite the substitutional nature of Ga insertion and the metallic nature of their mixture that should thoroughly delocalize and scramble the noncore electrons that bind the atoms together, is why we suggest that the Pu–Ga system is more of a “chemistry” than a “physics” problem.

Although the [Ga] independence of the EXAFS demonstrates that the Ga atoms avoid direct bonding and therefore appear to repel each other as nn, the only way we have found to duplicate this constancy of the Ga environment over a wide range of [Ga] is to assume that they nevertheless act cooperatively by attracting each other over longer distances. The results presented here are therefore most easily explained by invoking such an attractive interaction that peaks over a 4–6 Å range following a repulsive interaction at shorter distances that would originate in the lattice strain from their smaller size. This combination of distance-dependent repulsion and attraction would cause the Ga atoms to cluster and subsequently organize into a quasi-intermetallic of approximate composition  $\text{Pu}_{25\text{--}35}\text{Ga}$  with the Ga–Ga distances and angles exhibiting merely preferred rather than the precise values of a true intermetallic. The attractive force is also sufficiently weak so that the clustering only involves the Ga atoms within several nm of each other and within a single microcrystal or grain there are embedded many Ga-depleted domains. Complete segregation of the Ga across a micrometer scale grain and subsequent phase separation into separate crystals of  $\text{Pu}_{30}\text{Ga}$  and  $\alpha$  Pu do not occur.  $\text{Pu}_{30}\text{Ga}$  would therefore compete with randomly dispersed Ga and  $\text{Pu}_3\text{Ga} + \alpha$  Pu over at least some temperature range of the  $\delta$  region of the phase diagram. Crystals or grains of Pu–Ga will therefore be homogeneous  $\text{Pu}_{25\text{--}35}\text{Ga}$  when it saturates the material at around 3.5 atom % Ga. Below this 3.5 atom % Ga concentration the clustering of the Ga promotes the formation of nanoscale Ga-depleted regions analogous to a spinodal decomposition. Lacking Ga atoms to stabilize the  $\delta$  phase but unable to form  $\alpha$  Pu because of the tensile and epitaxial stress imposed by the  $\delta$  host, up to 20–25% of the Pu atoms that reside in these regions rearrange into the  $\sigma$  structure whose long-range average structure is also cubic, but 6–7% larger so that some interstitial atoms are required to maintain the density. In addition, there is the modulation that splits the nn Pu–Pu bonds into two sets at around 3.2–3.3 and 3.8 Å.<sup>93</sup> The former causes the shorter Pu–Pu bonds in  $\sigma$  to match those of  $\delta$ , which could be an epitaxial constraint, and their ratio with the longer ones is that of a bcc structure, which could be significant rather than merely coincidental. Larger domains of  $\sigma$  that occur in samples with compositions very close to the 1 atom % Ga lower limit of the  $\delta$  phase and with minimal additional impurities may further rearrange into a  $\sigma'$  structure that is more like  $\alpha$  Pu in that the bonds  $>3$  Å become disordered and the shorter ones around 2.6 Å involving the interstitial atoms locally order. Ga atoms are excluded from the  $\sigma$  structure but not from the larger domains in  $\sigma'$ , where they appear to reside in highly disordered environments that render them invisible in EXAFS, similar to what we have observed in the EXAFS of  $\alpha'$  Pu.

These collective and cooperative phenomena challenge not only our conceptual basis for the structural behavior of solid solutions but also our intuition with regard to experimental results and modeling. The most incisive example is the demonstration within the data presented here that a crystalline material can contain tens of percents of a second ordered structure that is clearly visible in local structure measurements

but that may not (or may) display a diffraction pattern accompanying that of the host, indicating the importance of the morphology of its domains on the nanometer scale. Motivated by this finding we discovered via modeling<sup>1,2,5–7,95</sup> that this is not a difficult feat. However, insofar as the concept of nanoscale heterogeneity and its origin in the collective behavior of defects in a host lattice is relatively new, a number of issues remain. These include modeling results based on other materials that indicate that the concentration of radiation-induced defects should be in the parts-per-thousand range, 1–2 orders of magnitude below what we observe. This discrepancy could occur simply because the modeling does not yet incorporate cooperative effects. Another is the absence of signatures in small angle scattering and TEM. The failure of small angle scattering to find the heterogeneity is also easy to explain; interstitials in the open  $\sigma$  structure render its density identical to that of the host  $\delta$  so that there is no contrast to produce a signal. We will comment on the microscopy below, but the crucial realization is that the scientific intuition developed from studies of simple materials cannot be extrapolated to complex ones and this extends even to such ostensibly elementary properties as whether an ordered structure does or does not give a diffraction pattern.

The structure:function relationships involved in the translation of the heterogeneity into other properties—especially bulk properties—are perhaps best understood by invoking latent or potential  $\sigma$  domains in addition to the expressed or actual ones we observe. A latent domain would be a Ga-depleted region that is pinned into the  $\delta$  structure under current conditions but that might rearrange into  $\sigma$  or even  $\sigma'$  in response to a modest change in temperature, pressure, etc. I.e., it is a local minimum in the energy landscape that is unoccupied because its energy for the atoms in that region is higher than if they are in the  $\delta$  structure, but the relative energies of the  $\sigma$  and  $\delta$  minima are so close that small perturbations can flip their order causing the atoms to transform to  $\sigma$ . Likewise, an expressed  $\sigma$  domain could just as easily be tipped into the  $\delta$  structure in the same way. The expressed and latent  $\sigma$  nanodomains will display a continuous range of stabilities with respect to  $\delta$ – $\sigma$  interconversion because of their continuous range of sizes, shapes, and interactions with the host. The continuous behaviors in bulk properties, e.g., density, hardness, elastic constants, etc., exhibited by  $\delta$ -stabilized Pu alloys through the heterogeneous–homogeneous transition and their sensitivity to the material's processing history therefore result from the plethora of these domains responding to the probe sequentially as their individual transformation thresholds are crossed rather than simultaneously; the response of these alloys to macroscopic effects is the sum of the individual responses of both the actual and potential structures of all the mesodomains. Although this process is neither the intent nor necessarily a consequence of the description of the electronic structure of Pu as a superposition of two valences<sup>74</sup> or of multiple more generic states,<sup>48,54,73,75</sup> it is nevertheless tempting to speculate that this structural instability in terms of two potentials originates in the coexistence of multiple electronic states whose relative contributions to the final electronic and crystal structure are affected by the local environment.

This coexistence of multiple structures in  $\delta$  Pu–Ga that constitute the smallest scale martensitic texture questions fundamental aspects of the martensitic transformation mechanism.<sup>81</sup> Is the rate-limiting step nucleation if static structures

related to the final phase are already present, or is the linking of these  $\alpha$ -like  $\sigma/\sigma'$  domains subject to the geometric constraints of the product within the host the critical factor?<sup>76,122</sup> Elastic response issues also suggest that caution must be exercised in interpreting results from other experiments, e.g., TEM, where the uniaxial nature of the samples may affect elastic phenomena so that static defects such as bubbles are retained whereas more sensitive ones such as dislocation loops<sup>123–125</sup> and heterogeneity may be modified in thin sections or in proximity to surfaces. Electron microscopy may also simply be insensitive to small or thin domains; the surface oxide that must be on the surface in TEM samples is typically not observed.

The collective behavior of Pu–Ga expressed as the Ga organization and heterogeneity is critical in the observed aging processes. The initial response to aging is the loss of the  $\sigma$  structure.<sup>27,28</sup> Subsequently, however, other specific lattice distortions occur, the exact details of which may depend on [Ga], the actual age, and the specifics of the sample fabrication and history. Ultimately, however, much of the midage order is lost and the material begins to appear amorphous on the 5–10 Å scale even as much of its long-range order is retained, either on average in that the displacements of atoms from their lattice sites cancel each other over large numbers or as conserved  $\delta$  domains in which the atoms are not displaced and reside on the lattice. Aging may have minor or delayed effects on the static components of the Debye–Waller factors but does appear to reduce the thermal component of the Pu–Pu bonds, i.e., their pair potentials become narrower. Aging effects on the width of the nn  $\delta$  Ga–Pu shell are significantly smaller than their observed composition dependence. It is possible that aging effects and the differences between samples due to their different histories may be comparable in extent. Insofar as calculations of  $\delta$ -stabilized Pu–Ga fail to find quasi-ordered Ga arrangements and heterogeneity, modeling of radiation-induced defects based on both Pu specific<sup>31,124,125</sup> and conventional<sup>29,124,126</sup> models that include only He bubbles and limited numbers of dislocations as the principal radiation effects certainly do not consider the possibility of Ga-organized accumulation of defects into novel structures occupying up to tens of percents of the crystal. These calculations are therefore unable to include, e.g., stabilization of the defects by the formation of ordered structures in Ga-depleted domains that most likely account for the preservation of the ordered  $\delta$  Pu lattice throughout the bulk of the crystal observed in diffraction and EXAFS. Thus, the atomic-scale mechanisms utilized by models that cannot incorporate collective behavior and heterogeneity as an intrinsic, continuous property of  $\delta$ -stabilized Pu–Ga will necessarily be incomplete.

These results suggest that the best explanation of the structure of  $\delta$ -stabilized/retained Pu alloys is via a total free energy landscape<sup>127</sup> that includes multiscale elastic (strongly interacting inhomogeneities) and entropic (finite  $K$ ) in addition to electronic (zero  $K$ ) contributions. However, instead of depicting the energies of a single molecule over all of its possible conformational states, an energy landscape for a crystalline solid could show the energy at a given temperature, pressure, etc., of an atom of a particular element as a function of local composition (or position). This becomes interesting in a complex crystalline solid where this atom may access two different conformations or species whose relative energies depend upon these local conditions (Figure 15). The local strain in proximity to inhomogeneities will raise nearby atoms' energies above the minimum for an undistorted crystal, altering

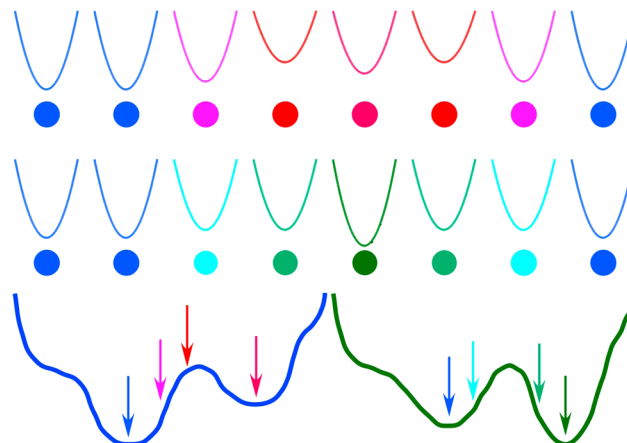


**Figure 15.** Top: Atoms (circles, their individual potentials are curves above them) in a domain (red, magenta) with a local composition that deviates significantly from the average not only have higher energies than the atoms residing in defect-free portions of the host lattice (blue) but also strain their neighboring atoms and raise their energies (purple). After relaxation by displacing atoms to attain the lowest total free energy for this conformation, the resulting energy landscape (lower left, energy plotted as a function of local composition, not position) shows the domain center in a local minimum that is higher than that of the perfect crystal and the strained atoms on unstable regions. If, however, the atoms in the domain possess multiple states/conformations, reconfiguration or rehybridization accompanied by transformation of its domain into a different structural motif can lower their energy in the crystal (middle, dark green) and shift the total energy of the rearranged domain below the original one derived from the host lattice. The result will be a heterogeneous material exhibiting multiple ordered structures, the expression of which depends upon the local composition. Functionality is coupled to this landscape via conformational changes effected by the application of both homogeneous state variables such as temperature or magnetic field and local composition changes resulting from, e.g., binding small molecules.

the landscape from the simple potential of a pure material and even producing new chemical species. Heterogeneity will result when the deviations from the global average in local composition and environment for a set of atoms are sufficiently large to shift the energy of the second conformation below that of the original one.<sup>84</sup> Or, if recent calculations involving superpositions of multiple configurations/valences are the right approach, heterogeneity will result from different admixtures of quantum states that result from these same parameters.<sup>74</sup> An essential aspect of this landscape is that it is dynamic in that it is subject to modifications that alter its relative energies and therefore the mesoscale structure of the material. Extrinsic homogeneous variables, e.g., temperature, pressure, magnetic fields, etc., will raise or lower the curves by different amounts at different locations depending on the local response and thus tip the balance between the various structures or even produce new ones. This intrinsic nanoscience underlies the functionality of complex materials.

The essential factor differentiating this real Pu–Ga landscape from the ideal simple symmetric one of homogeneous, entropically stabilized  $\delta$  Pu(Ga)<sup>82–85</sup> in which all of the atoms are equivalent is the local effects of the “impurities”. These would be the Ga that stabilize the  $\delta$  structure, but as this work has indicated it would also include the large number of radiation induced defects that accumulate with time. The competing electronic structures of Pu and their coupling to

different arrangements of atoms support the suggestion that stabilized  $\delta$  Pu exhibits quantum criticality.<sup>47,65,120</sup> The electronic structure of Pu, and most especially  $\delta$  Pu and  $\delta$ -stabilized Pu alloys, continues to be one of the more significant challenges in electronic structure calculations.<sup>31,38,39,43–46,49–51,53–60,62–64,67,73,82,92,120,122,128–141</sup> At this moment, although there is now renewed agreement that it is not magnetic,<sup>68–71</sup> there is none on the best approach, with recent reports involving refining the inputs for more conventional descriptions,<sup>70,71</sup> electronic anisotropy,<sup>67</sup> and fluctuating valence.<sup>74</sup> Although there is consensus that the ambiguity of Pu is caused by the relative instability within the f bands, the various approaches differ on the mechanism by and extent to which the f electrons are localized in the  $\delta$  phase. The idea that it results from a delicate balance of opposing electronic characteristics<sup>139</sup> that point to the refined application of more conventional descriptions of the electronic structure<sup>70,71</sup> is inconsistent with the absence of significant change in f occupancy despite substantial changes in atom size in fcc Pu–Am alloys. The alternative described here, intermediate electron–phonon coupling giving multiple local minima in the potential surface that are rendered more stable by cooperative structural rearrangement of domains whose local compositions have deviated from the average,<sup>128</sup> perhaps supplemented by differential anisotropy in the Pu–Pu and Ga–Pu bonding<sup>67</sup> and an admixture of quantum states,<sup>74</sup> may be better. The collective aspects are apparent in the fact that the important structures in  $\delta$  Pu–Ga are larger scale ones associated with transformations; it has been shown that the anomalies in the phonons and associated shear moduli are coupled to the higher temperature phonons associated with structural transitions.<sup>141</sup>

## CONCLUSIONS

As often happens with complex materials, both overall and element-specific local structure experiments give a very much different description of the structure of Pu–Ga alloys and the effects of their self-irradiation than more conventional crystallographic approaches. In this regard it is important to remember, first, that  $\delta$  Pu–Ga alloys are kinetically trapped with respect to their more stable separation into  $\alpha$  Pu and  $\text{Pu}_3\text{Ga}$ <sup>39</sup> and some of these observed behaviors could result from the materials being in nonequilibrium forms, and, second, that these measurements with mm size probe beams are averaging any inhomogeneities in composition and structure that can occur in Pu–Ga on the 10–100  $\mu\text{m}$  scale of the grains. This uncertainty that is a major contribution to the variations in the EXAFS coupled to the precise composition and preparation process, in combination with the difficulties of quantifying the EXAFS of an anharmonically disordered material, is why we have presented these results in a qualitative rather than quantitative way. Independent EXAFS and pdf data corroborate each other in identifying and describing a novel Pu structure that may correspond to that of pure Pu under negative (tensile) pressure. In these alloys this  $\sigma$  Pu forms in the Ga-depleted regions that occur as a consequence of the self-organization of the Ga into  $\text{Pu}_{25–35}\text{Ga}$  domains below the ~3.3 atom %  $\text{Pu}_{25–35}\text{Ga}$  saturation limit that also is the upper bound for alloys that are metastable with respect to the martensitic transformation to  $\alpha$ – $\delta$  mixtures. The Ga-depleted domains that would form  $\alpha$  Pu in isolation are embedded in the  $\delta$  host, where epitaxial constraints cause the formation of  $\sigma$  Pu. These same constraints then dictate a conservation of the density as well as a particular pattern of bond lengths, with the overall behavior perhaps

reflecting the unusual structural and bonding properties of Pu that are also manifested in its phase diagram. Metastable  $\delta$  Pu–Ga is therefore an example of a system that exhibits nanoscale heterogeneity, i.e., it is composed of coexisting ordered structures in which the domain size of the minority one is at or below the diffraction limit. Under certain conditions the  $\sigma$  Pu forms in such a way that it does give diffraction patterns that are consistent with the local structure results. This same phenomenon is also a crucial property of aged materials in which local structure measurements identify additional types of ordered structures. These would also result from the clustering of defects that, either separately or together with the Ga or other minor elements, aggregate to form domains at or below the diffraction limit in size that rearrange into non- $\delta$  structures. Their inert character and resistance to defect recombination might be intrinsic, but it is also possible that these structures involving radiation-induced defects are stabilized on the  $\delta$ – $\sigma$  or other types of interfaces in the material. The collective and cooperative behavior that are the origin of these effects can be explained within the context of a dynamic energy landscape in which the conformation or geometry of the atoms has access to two or more forms, with the relative energies of these local minima varying depending on the local composition.

## AUTHOR INFORMATION

### Corresponding Author

\*Tel: (505) 667-9584. Fax: (505) 667-8021. E-mail: conradson@lanl.gov.

### Notes

The authors declare no competing financial interest.

## ACKNOWLEDGMENTS

Interpretation of the data was supported by the Heavy Element Chemistry Program, Chemical Sciences, Biosciences, and Geosciences Division, Office of Basic Energy Sciences; measurements and analysis by the Enhanced Surveillance Campaign, National Nuclear Security Administration. Los Alamos National Laboratory is operated by Los Alamos National Security, LLC, for the National Nuclear Security Administration of U.S. Department of Energy under Contract DEAC52-06NA25396. XAFS and XRD were performed at SSRL (Stanford Linear Accelerator Center) and APS (Argonne National Laboratory), which are operated by the US Department of Energy, Office of Basic Energy Sciences. MRCAT and PNC-CAT operations are supported by the member institutions. Health Physics operations at SSRL and APS were supported by the Seaborg Institute for Transactinium Science at LANL. We thank Angus Lawson for analysis of supporting diffraction data. A.J.G.-A. thanks the Spanish MICINN for financial support under the I+D+i programme (Grant FIS2009-14293).

## REFERENCES

- (1) Dimitrov, D. A.; Bishop, A. R.; Conradson, S. D. Crystallography of a Two-Dimensional Binary Crystal with Local Distortions. *Phys. Rev. B* **1997**, *56*, 2969–2976.
- (2) Dimitrov, D. A.; Ankudinov, A. L.; Bishop, A. R.; Conradson, S. D. Pair Distribution Function and X-Ray Absorption Signatures of Rotational and Radial Local Distortions in a Model System with Average Long-Range Order. *Phys. Rev. B* **1998**, *58*, 14227–14237.
- (3) Conradson, S. D.; Espinosa, F. J.; Henderson, A.; Villegas, P. M. In *International Symposium on Physics in Local Lattice Distortions*

- (LLD2K); Oyanagi, H.; Bianconi, A., Eds.; AIP: Tsukuba, Japan, 2000; Vol. 554, pp 503–511.
- (4) Proffen, T.; Billinge, S. J. L.; Egami, T.; Louca, D. Structural Analysis of Complex Materials Using the Atomic Pair Distribution Function - A Practical Guide. *Z. Kristallogr.* **2003**, *218*, 132–143.
- (5) Garcia-Adeva, A. J.; Conradson, D. R.; Villegas, P.; Conradson, S. D. Signatures of Collective Local and Nanoscale Distortions in Diffraction Experiments. *J. Phys. Chem. B* **2003**, *107*, 6704–6716.
- (6) Howell, R. C.; Conradson, S. D.; Garcia-Adeva, A. J. Coherent Versus Uncorrelated Nanoscale Heterogeneities in L10 Solid Solutions and Their Signatures from Local and Extended Probes. *J. Phys. Chem. B* **2006**, *111*, 159–167.
- (7) Andersson, D. A.; Casillas, L.; Baskes, M. I.; Lezama, J. S.; Conradson, S. D. Modeling of the Phase Evolution in  $Mg_{1-x}Al_xB_2$  ( $0 < x < 0.5$ ) and its Experimental Signatures. *J. Phys. Chem. B* **2009**, *113*, 11965–11976.
- (8) Conradson, S. D. Application of X-Ray Absorption Fine Structure Spectroscopy to Materials And Environmental Science. *Appl. Spectrosc.* **1998**, *52*, 7565–7576.
- (9) Conradson, S. D. In *Challenges in Plutonium Science*; Cooper, N. G., Ed.; Los Alamos National Laboratory: Los Alamos, New Mexico, USA, 2000; Vol. 26, pp 356–363.
- (10) Kuch, W.; Parkin, S. S. P. Fe Structural and Magnetic Phases in Fe/Ni<sub>81</sub>Fe<sub>19</sub>(001) Multilayers. *Europhys. Lett.* **1997**, *37*, 465–470.
- (11) Kuch, W.; Parkin, S. S. P. Structural and Magnetic Phases of Fe in Fe/Ni(0 0 1) and Fe/Ni<sub>81</sub>Fe<sub>19</sub>(0 0 1) Multilayers. *J. Magn. Magn. Mater.* **1998**, *184*, 127–136.
- (12) Biedermann, A.; Tschelissnig, R.; Klein, C.; Schmid, M.; Varga, P. Reconstruction of the Clean and H Covered “Magnetic Live Surface Layer” of Fe Films Grown on Cu(100). *Surf. Sci.* **2004**, *563*, 110–126.
- (13) Biedermann, A.; Tschelissnig, R.; Schmid, M.; Varga, P. Local Atomic Structure of Ultra-Thin Fe Films Grown on Cu(100). *Appl. Phys. A* **2004**, *78*, 807–816.
- (14) Horovitz, B.; Barsch, G. R.; Krumhansl, J. A. Twin Bands in Martensites - Statics and Dynamics. *Phys. Rev. B* **1991**, *43*, 1021–1033.
- (15) Kartha, S.; Castan, T.; Krumhansl, J. A.; Sethna, J. P. Spin-Glass Nature of Tweed Precursors in Martensitic Transformations. *Phys. Rev. Lett.* **1991**, *67*, 3630–3633.
- (16) Kartha, S.; Krumhansl, J. A.; Sethna, J. P.; Wickham, L. K. Disorder-Driven Pretransitional Tweed Pattern in Martensitic Transformations. *Phys. Rev. B* **1995**, *52*, 803–822.
- (17) Krumhansl, J. A. Viewpoints on Microscopic and Mesoscopic Transformation Processes in Martensite. *J. Phys. IV* **1995**, *5*, 3–14.
- (18) Krumhansl, J. A. Microscience of Transforming Materials: Simple to Distributed Defect Models. *Phase Transitions* **1999**, *69*, 395–407.
- (19) Krumhansl, J. A. Multiscale Science: Materials in the 21st Century. In *Materials Science Forum Series #327*; Saburi, T., Ed.; Trans Tech Publications: Durnten-Zurich Switzerland, **2000**; pp 1–7.
- (20) Bishop, A. R.; Lookman, T.; Saxena, A.; Shenoy, S. R. Elasticity-Driven Nanoscale Texturing in Complex Electronic Materials. *Europhys. Lett.* **2003**, *63*, 289–295.
- (21) Saxena, A.; Wu, Y.; Lookman, T.; Shenoy, S. R.; Bishop, A. R. Hierarchical Pattern Formation in Elastic Materials. *Physica A* **1997**, *239*, 18–34.
- (22) Shenoy, S. R.; Lookman, T.; Saxena, A.; Bishop, A. R. Martensitic Textures: Multiscale Consequences of Elastic Compatibility. *Phys. Rev. B* **1999**, *60*, R12537–R12541.
- (23) Rasmussen, K. O.; Lookman, T.; Saxena, A.; Bishop, A. R.; Albers, R. C.; Shenoy, S. R. Three-Dimensional Elastic Compatibility and Varieties of Twins In Martensites. *Phys. Rev. Lett.* **2001**, *87*, 055704.
- (24) Klein, W.; Lookman, T.; Saxena, A.; Hatch, D. M. Nucleation in Systems with Elastic Forces. *Phys. Rev. Lett.* **2002**, *88*, 085701.
- (25) Ahluwalia, R.; Lookman, T.; Saxena, A.; Albers, R. C. Landau Theory for Shape Memory Polycrystals. *Acta Mater.* **2004**, *52*, 209–218.
- (26) Gagne, C. J.; Gould, H.; Klein, W.; Lookman, T.; Saxena, A. Simulations of Spinodal Nucleation in Systems with Elastic Interactions. *Phys. Rev. Lett.* **2005**, *95*, 095701.
- (27) Drell, S.; Jeanloz, R.; Peurifoy, B. Maintaining a Nuclear Deterrent Under the Test Ban Treaty. *Science* **1999**, *283*, 1119–1120.
- (28) Jeanloz, R. Science-Based Stockpile Stewardship. *Phys. Today* **2000**, *53*, 44–50.
- (29) Wirth, B. D.; Schwartz, A. J.; Fluss, M. J.; Caturia, M. J.; Wall, M. A.; Wolfer, W. G. Fundamental Studies of Plutonium Aging. *MRS Bull.* **2001**, *26*, 679–683.
- (30) Fluss, M. J.; Wirth, B. D.; Wall, M.; Felter, T. E.; Caturia, M. J.; Kubota, A.; de la Rubia, T. D. Temperature-Dependent Defect Properties From Ion-Irradiation in Pu(Ga). *J. Alloys Compd.* **2004**, *368*, 62–74.
- (31) Valone, S. M.; Baskes, M. I.; Stan, M.; Mitchell, T. E.; Lawson, A. C.; Sickafus, K. E. Simulations of Low Energy Cascades in fcc Pu Metal at 300 K and Constant Volume. *J. Nucl. Mater.* **2004**, *324*, 41–51.
- (32) Chung, B. W.; Schwartz, A. J.; Ebbinghaus, B. B.; Fluss, M. J.; Haslam, J. J.; Blobaum, K. J. M.; Tobin, J. G. Spectroscopic Signature of Aging in delta-Pu(Ga). *J. Phys. Soc. Jpn.* **2006**, *75*, 054710.
- (33) Chung, B. W.; Thompson, S. R.; Woods, C. H.; Hopkins, D. J.; Gourdin, W. H.; Ebbinghaus, B. B. Density Changes in Plutonium Observed from Accelerated Aging Using Pu-238 Enrichment. *J. Nucl. Mater.* **2006**, *355*, 142–149.
- (34) Valone, S. M.; Baskes, M. I.; Martin, R. L. Atomistic Model of Helium Bubbles in Gallium-Stabilized Plutonium Alloys. *Phys. Rev. B* **2006**, *73*, 214209.
- (35) McCall, S. K.; Fluss, M. J.; Chung, B. W.; McElfresh, M. W.; Jackson, D. D.; Chapline, G. F. Emergent Magnetic Moments Produced by Self-Damage in Plutonium. *Proc. Natl. Acad. Sci. U.S.A.* **2006**, *103*, 17179–17183.
- (36) Booth, C. H.; Jiang, Y.; Medling, S. A.; Wang, D. L.; Costello, A. L.; Schwartz, D. S.; Mitchell, J. N.; Tobash, P. H.; Bauer, E. D.; McCall, S. K.; et al. Self-irradiation Damage to the Local Structure of Plutonium and Plutonium Intermetallics. *J. Appl. Phys.* **2013**, *113*, 093502.
- (37) Lander, G. H. Sensing Electrons on the Edge. *Science* **2003**, *301*, 1057–1059.
- (38) Hecker, S. S. The Magic of Plutonium: 5f Electrons and Phase Instability. *Metall. Trans. A* **2004**, *35A*, 2207–2222.
- (39) Hecker, S. S.; Harbur, D. R.; Zocco, T. G. Phase Stability and Phase Transformations in Pu-Ga Alloys. *Prog. Mater. Sci.* **2004**, *49*, 429–485.
- (40) Schwartz, A. J. Plutonium Metallurgy: The Materials Science Challenges Bridging Condensed-Matter Physics and Chemistry. *J. Alloys Compd.* **2007**, *444*, 4–10.
- (41) Baskes, M. I.; Hu, S. Y.; Valone, S. M.; Wang, G. F.; Lawson, A. C. Atomistic Simulations of Ga Atom Ordering in Pu 5 at. % Ga Alloys. *J. Comput.-Aided Mater. Des.* **2007**, *14*, 379–388.
- (42) Hu, S. Y.; Baskes, M. I.; Stan, M.; Mitchell, J. N.; Zhang, J. X.; Chen, L. Q. Effect of Elastic Anisotropy and Inhomogeneity on Coring Structure Evolution in Pu-Ga Alloys - Phase-Field Modeling. *J. Comput.-Aided Mater. Des.* **2007**, *14*, 389–402.
- (43) Nordstrom, L.; Wills, J. M.; Andersson, P. H.; Soderlind, P.; Eriksson, O. Spin-Orbit Coupling in the Actinide Elements: A Critical Evaluation of Theoretical Equilibrium Volumes. *Phys. Rev. B* **2001**, *63*, 035103/1–5.
- (44) Savrasov, S. Y.; Kotliar, G.; Abrahams, E. Correlated Electrons in delta -Plutonium Within a Dynamical Mean-Field Picture. *Nature* **2001**, *410*, 793–795.
- (45) Havela, L.; Gouder, T.; Wastin, F.; Rebizant, J. Photoelectron Spectroscopy Study of the 5f Localization in Pu. *Phys. Rev. B* **2002**, *65*, 235118/1–9.
- (46) Landa, A.; Soderlind, P.; Ruban, A. Monte Carlo Simulations of the Stability of delta-Pu. *J. Phys.: Condens. Matter* **2003**, *15*, L371–L376.
- (47) Lashley, J. C.; Singleton, J.; Migliori, A.; Betts, J. B.; Fisher, R. A.; Smith, J. L.; McQueeney, R. J. Experimental Electronic Heat

- Capacities of alpha- and delta-Plutonium: Heavy-Fermion Physics in an Element. *Phys. Rev. Lett.* **2003**, *91*, 205901/1–4.
- (48) Lawson, A. C.; Roberts, J. A.; Martinez, B.; Richardson, J. W.; Ledbetter, H.; Migliori, A. Applying the Two-State Invar Model to delta-Phase Plutonium. *JOM* **2003**, *55*, 31–33.
- (49) Sadigh, B.; Soderlind, P.; Wolfer, W. G. Geometry and Electronic Structure of alpha-Pu: A Theoretical Study. *Phys. Rev. B* **2003**, *68*, 241101.
- (50) Tobin, J. G.; Chung, B. W.; Schulze, R. K.; Terry, J.; Farr, J. D.; Shuh, D. K.; Heinzelman, K.; Rotenberg, E.; Waddill, G. D.; van der Laan, G. Resonant Photoemission in f-Electron Systems: Pu and Gd. *Phys. Rev. B* **2003**, *68*, 155109.
- (51) Kotliar, G.; Vollhardt, D. Strongly Correlated Materials: Insights From Dynamical Mean-Field Theory. *Phys. Today* **2004**, *57*, 53–59.
- (52) Landa, A.; Soderlind, P. First-Principles Calculations of Stability of delta-Pu-Am Alloys. *J. Alloys Compd.* **2004**, *376*, 6704–6716.
- (53) Soderlind, P.; Sadigh, B. Density-Functional Calculations of alpha, beta, gamma, delta, delta', and epsilon Plutonium. *Phys. Rev. Lett.* **2004**, *92*, 185702/1–4.
- (54) Wills, J. M.; Eriksson, O.; Delin, A.; Andersson, P. H.; Joyce, J.; Durakiewicz, T.; Butterfield, M. T.; Arko, A. J.; Moore, D. P.; Morales, L. A. A Novel Electronic Configuration of the 5f States in delta-Plutonium as Revealed by the Photo-Electron Spectra. *J. Electron Spectrosc. Relat. Phenom.* **2004**, *135*, 163–166.
- (55) Graf, M. J.; Lookman, T.; Wills, J. M.; Wallace, D. C.; Lashley, J. C. Strong Electron-Phonon Coupling in delta-Phase Stabilized Pu. *Phys. Rev. B* **2005**, *72*, 045135.
- (56) Lashley, J. C.; Lawson, A. C.; McQueeney, R. J.; Lander, G. H. Absence of Magnetic Moments in Plutonium. *Phys. Rev. B* **2005**, *72*, 054416.
- (57) Piskunov, Y.; Mikhalev, K.; Geraschenko, A.; Pogudin, A.; Ogloblichev, V.; Verkhosvskii, S.; Tankeyev, A.; Arkhipov, V.; Zouev, Y.; Lekomtsev, S. Spin Susceptibility of Ga-Stabilized delta-Pu Probed by Ga-69 NMR. *Phys. Rev. B* **2005**, *71*, 174401.
- (58) Shick, A. B.; Drchal, V.; Havela, L. Coulomb-U and Magnetic-Moment Collapse in delta-Pu. *Europhys. Lett.* **2005**, *69*, 588–594.
- (59) Shorikov, A. O.; Lukyanov, A. V.; Korotin, M. A.; Anisimov, V. I. Magnetic State and Electronic Structure of the Delta and Alpha Phases of Metallic Pu and its Compounds. *Phys. Rev. B* **2005**, *72*, 024458.
- (60) Tobin, J. G.; Moore, K. T.; Chung, B. W.; Wall, M. A.; Schwartz, A. J.; van der Laan, G.; Kutepov, A. L. Competition Between Delocalization and Spin-Orbit Splitting in the Actinide 5f States. *Phys. Rev. B* **2005**, *72*, 085109.
- (61) Lawson, A. C.; Roberts, J. A.; Martinez, B.; Ramos, M.; Kotliar, G.; Trouw, F. W.; Fitzsimmons, M. R.; Hehlen, M. P.; Lashley, J. C.; Ledbetter, H.; et al. Invar Model for delta-Phase Pu: Thermal Expansion, Elastic and Magnetic Properties. *Philos. Mag.* **2006**, *86*, 2713–2733.
- (62) Moore, K. T.; Soderlind, P.; Schwartz, A. J.; Laughlin, D. E. Symmetry and Stability of delta Plutonium: The Influence of Electronic Structure. *Phys. Rev. Lett.* **2006**, *96*, 206402/1–4.
- (63) Moore, K. T.; van der Laan, G.; Tobin, J. G.; Chung, B. W.; Wall, M. A.; Schwartz, A. J. Probing the Population of the Spin-Orbit Split Levels in the Actinide 5f States. *Ultramicroscopy* **2006**, *106*, 261–268.
- (64) Pourovskii, L. V.; Katsnelson, M. I.; Lichtenstein, A. I.; Havela, L.; Gouder, T.; Wastin, F.; Shick, A. B.; Drchal, V.; Lander, G. H. Nature of Non-Magnetic Strongly-Correlated State in delta-Plutonium. *Europhys. Lett.* **2006**, *74*, 479–485.
- (65) Chapline, G.; Fluss, M.; McCall, S. Plutonium and Quantum Criticality. *J. Alloys Compd.* **2007**, *444*, 142–144.
- (66) Heffner, R. H.; Ohishi, K.; Fluss, M. J.; Morris, G. D.; MacLaughlin, D. E.; Shu, L.; Chung, B. W.; McCall, S. K.; Bauer, E. D.; Sarrao, J. L.; et al. The Search for Magnetic Order in delta-Pu Metal Using Muon Spin Relaxation. *J. Alloys Compd.* **2007**, *444*, 80–83.
- (67) Moore, K. T.; Laughlin, D. E.; Soderlind, P.; Schwartz, A. J. Incorporating Anisotropic Electronic Structure in Crystallographic Determination of Complex Metals: Iron And Plutonium. *Philos. Mag.* **2007**, *87*, 2571–2588.
- (68) Tobin, J. G.; Soderlind, P.; Landa, A.; Moore, K. T.; Schwartz, A. J.; Chung, B. W.; Wall, M. A.; Wills, J. M.; Haire, R. G.; Kutepov, A. L. On the Electronic Configuration in Pu: Spectroscopy and Theory. *J. Phys.: Condens. Matter* **2007**, *20*, 125204–125212.
- (69) Zhu, J. X.; McMahan, A. K.; Jones, M. D.; Durakiewicz, T.; Joyce, J. J.; Wills, J. M.; Albers, R. C. Spectral Properties of delta-Plutonium: Sensitivity to 5f Occupancy. *Phys. Rev. B* **2007**, *76*, 245118.
- (70) Julien, J. P.; Zhu, J. X.; Albers, R. C. Coulomb Correlation in the Presence of Spin-Orbit Coupling: Application to Plutonium. *Phys. Rev. B* **2008**, *77*, 195123.
- (71) Soderlind, P. Quantifying the Importance of Orbital Over Spin Correlations in delta-Pu Within Density-Functional Theory. *Phys. Rev. B* **2008**, *77*, 085101/1–5.
- (72) Yin, Q.; Kutepov, A.; Haule, K.; Kotliar, G.; Savrasov, S. Y.; Pickett, W. E. Electronic Correlation and Transport Properties of Nuclear Fuel Materials. *Phys. Rev. B* **2011**, *84*, 195111/1–7.
- (73) Joyce, J. J.; Wills, J. M.; Durakiewicz, T.; Butterfield, M. T.; Guziewicz, E.; Moore, D. P.; Sarrao, J. L.; Morales, L. A.; Arko, A. J.; Eriksson, O.; et al. Dual nature of the 5f Electrons in Plutonium Materials. *Physica B* **2006**, *378–380*, 920–924.
- (74) Shim, J. H.; Kotliar, G.; Haule, K. Fluctuating Valence in a Correlated Solid and the Anomalous Properties of delta-Plutonium. *Nature* **2007**, *446*, 513–516.
- (75) Booth, C. H.; Jiang, Y.; Wang, D. L.; Mitchell, J. N.; Tobash, P. H.; Bauer, E. D.; Wall, M. A.; Allen, P. G.; Sokaras, D.; Nordlund, D.; et al. Multiconfigurational Nature of 5f Orbitals in Uranium and Plutonium Intermetallics. *Proc. Natl. Acad. Sci. U.S.A.* **2012**, *109*, 10205–10209.
- (76) Jin, Y. M.; Wang, Y. U.; Khachaturyan, A. G.; Krenn, C. R.; Schwartz, A. J. Crystallography of the delta → alpha Martensitic Transformation in Plutonium Alloys. *Metall. Mater. Trans. A* **2005**, *36A*, 2031–2047.
- (77) Blobaum, K. J. M.; Krenn, C. R.; Wall, M. A.; Massalski, T. B.; Schwartz, A. J. Nucleation and Growth of the alpha' Martensitic Phase in Pu-Ga Alloys. *Acta Mater.* **2006**, *54*, 4001–4011.
- (78) Hirth, J. P.; Mitchell, J. N.; Schwartz, D. S.; Mitchell, T. E. On the fcc → Monoclinic Martensite Transformation in a Pu-1.7 at.% Ga Alloy. *Acta Mater.* **2006**, *54*, 1917–1925.
- (79) Zocco, T. G.; Schwartz, D. S.; Park, J. Investigation of Plutonium Allotropic Phase Transformations Through Differential Scanning Calorimetry. *J. Nucl. Mater.* **2006**, *353*, 199–126.
- (80) Lookman, T.; Saxena, A.; Albers, R. C. Phonon Mechanisms and Transformation Paths in Pu. *Phys. Rev. Lett.* **2008**, *100*, 145504.
- (81) Xu, R. Q.; Wong, J.; Zschack, P.; Hong, H.; Chiang, T. C. Soft Phonons in delta-Phase Plutonium Near the delta-alpha' Transition. *EPL* **2008**, *83*, 26001/1–5.
- (82) Dai, X.; Savrasov, S. Y.; Kotliar, G.; Migliori, A.; Ledbetter, H.; Abrahams, E. Calculated Phonon Spectra of Plutonium at High Temperatures. *Science* **2003**, *300*, 953–956.
- (83) Wong, J.; Krisch, M.; Farber, D. L.; Occelli, F.; Schwartz, A. J.; Chiang, T. C.; Wall, M. A.; Boro, C.; Xu, R. Q. Phonon Dispersions of fcc delta-Plutonium-Gallium by Inelastic X-Ray Scattering. *Science* **2003**, *301*, 1078–1080.
- (84) McQueeney, R. J.; Lawson, A. C.; Migliori, A.; Kelley, T. M.; Ramos, M.; Martinez, B.; Lashley, J. C.; Vogel, S. C. Unusual Phonon Softening in delta-Phase Plutonium. *Phys. Rev. Lett.* **2004**, *92*, 146401/1–4.
- (85) Wong, J.; Krisch, M.; Farber, D. L.; Occelli, F.; Xu, R.; Chiang, T. C.; Clatterbuck, D.; Schwartz, A. J.; Wall, M. A.; Boro, C. Crystal Dynamics of delta fcc Pu-Ga Alloy by High-Resolution Inelastic X-Ray Scattering. *Phys. Rev. B* **2005**, *72*, 064115.
- (86) Cox, L. E.; Martinez, R.; Nickel, J. H.; Conradson, S. D.; Allen, P. G. Short-Range Atomic Structure of 1 Wt.% Ga Delta -Stabilized Plutonium by X-Ray-Absorption Fine-Structure Spectroscopy. *Phys. Rev. B* **1995**, *51*, 751–755.
- (87) Faure, P.; Deslandes, B.; Bazin, D.; Taillard, C.; Doukhan, R.; Fournier, J. M.; Falange, A. Lattice Collapse Around Gallium in PuGa

- Alloys as Revealed By X-Ray Absorption Spectroscopy. *J. Alloys Compd.* **1996**, *244*, 131–139.
- (88) Richard, N.; Faure, P.; Rofidal, P.; Truffier, J. L.; Bazin, D. PuGa Alloys: An X-ray Absorption Study. *J. Alloys Compd.* **1998**, *271*–273, 879–881.
- (89) Dormeval, M.; Valot, C.; Baclet, N. X Ray Diffraction Investigation of Pu-Ce and Pu-Ce-Ga Alloys Stabilized in the Delta-Phase. *J. Phys. IV* **2000**, *10*, 425–433.
- (90) Allen, P. G.; Henderson, A. L.; Sylwester, E. R.; Turchi, P. E. A.; Shen, T. H.; Gallegos, G. F.; Booth, C. H. Vibrational Properties of Ga-Stabilized delta -Pu by Extended X-Ray Absorption Fine Structure. *Phys. Rev. B* **2002**, *65*, 214107/1–7.
- (91) Nelson, E. J.; Blobaum, K. J. M.; Wall, M. A.; Allen, P. G.; Schwartz, A. J.; Booth, C. H. Local Structure and Vibrational Properties of alpha'-Pu Martensite in Ga-Stabilized delta-Pu. *Phys. Rev. B* **2003**, *67*, 224206.
- (92) Dormeval, M.; Baclet, N.; Valot, C.; Rofidal, P.; Fournier, J. M. Crystalline and Electronic Structure of Pu-Ce and Pu-Ce-Ga Alloys Stabilized in the Delta Phase. *J. Alloys Compd.* **2003**, *350*, 86–94.
- (93) Conradson, S. D.; Bock, N.; Castro, J. M.; Conradson, D. R.; Cox, L. E.; Dmowski, W.; Dooley, D. E.; Egami, T.; Espinosa-Faller, F. J.; Freibert, F.; et al. Nanoscale Heterogeneity, Pre-Martensitic Nucleation, and a Novel Plutonium Structure in Metastable delta fcc Pu-Ga Alloys. *Phys. Rev. B* **2014**, submitted.
- (94) Nelson, E. J.; Allen, P. G.; Blobaum, K. J. M.; Wall, M. A.; Booth, C. H. In *Actinides 2005-Basic Science, Applications and Technology*; Sarrao, J. L., Schwartz, A. J., Antonio, M. R., Burns, P. C., Haire, R. G., Nitsche, H., Eds.; Materials Research Society: Warrendale, PA, **2006**; Vol. 893, pp 109–114.
- (95) Espinosa-Faller, F. J.; Howell, R. C.; Garcia-Adeva, A. J.; Conradson, S. D.; Ignatov, A. Y.; Tyson, T. A.; Farrow, R. F. C.; Toney, M. F. Local Atomic Structure of Partially Ordered NiIn in NiMn/NiFe Exchange Coupled Layers: 1. XAFS Measurements and Structural Refinement. *J. Phys. Chem. B* **2005**, *109*, 10406–10418.
- (96) Tranquada, J. M.; Sternlieb, B. J.; Axe, J. D.; Nakamura, Y.; Uchida, S. Evidence for Stripe Correlations of Spins and Holes in Copper Oxide Superconductors. *Nature* **1995**, *375*, 561–563.
- (97) Bianconi, A.; Saini, N. L.; Rossetti, T.; Lanzara, A.; Perali, A.; Missori, M.; Oyanagi, H.; Yamaguchi, H.; Nishihara, Y.; Ha, D. H. Stripe Structure in the CuO<sub>2</sub> Plane Of Perovskite Superconductors. *Phys. Rev. B* **1996**, *54*, 12018–12021.
- (98) Bussmann-Holder, A.; Simon, A.; Buttner, H.; Bishop, A. R. Phonon Induced Stripe Formation and Charge Ordering in High-T<sub>c</sub> Superconductors. *Philos. Mag. B* **2000**, *80*, 1955–1960.
- (99) Dagotto, E.; Hotta, T.; Moreo, A. Colossal Magnetoresistant Materials: The Key Role of Phase Separation. *Phys. Rep.* **2001**, *344*, 1–153.
- (100) McElroy, K.; Lee, J.; Siezak, J. A.; Lee, D. H.; Eisaki, H.; Uchida, S.; Davis, J. C. Atomic-Scale Sources and Mechanism of Nanoscale Electronic Disorder in Bi<sub>2</sub>Sr<sub>2</sub>CaCu<sub>2</sub>O<sub>8+delta</sub>. *Science* **2005**, *309*, 1048–1052.
- (101) Lynn, J. E.; Kwei, G. H.; Trela, W. J.; Yuan, V. W.; Cort, B.; Martinez, R. J.; Vigil, F. A. Vibrational Properties of Pu and Ga in a Pu-Ga Alloy from Neutron-Resonance Doppler Spectroscopy. *Phys. Rev. B* **1998**, *58*, 11408–11415.
- (102) Lawson, A. C.; Roberts, J. A.; Martinez, B.; Von Dreele, R. B.; Storey, B.; Hawkins, H. T.; Ramos, M.; Hampel, F. G.; Davis, C. C.; Pereyra, R. A.; et al. Lattice Constants and Anisotropic Microstrain at Low Temperature in Pu-242-Ga Alloys. *Philos. Mag.* **2005**, *85*, 2007–2022.
- (103) Lashley, J. C.; Migliori, A.; Singleton, J.; McQueeney, R. J.; Blau, M. S.; Pereyra, R. A.; Smith, J. L. The Electron Heat Capacity of High-Purity alpha and Stabilized-delta Plutonium. *JOM* **2003**, *55*, 34–37.
- (104) Piskunov, Y.; Mikhalev, K.; Zuev, Y.; Verkhosvskii, S.; Arkhipov, V.; Svyatov, I.; Podgornova, I.; Shestakov, A.; Oglloblichev, V.; Pogudin, A.; et al. Ga-69 NMR in Pu<sub>1-x</sub>Ga<sub>x</sub> ( $x < 0.01$ ) Alloy. *J. Alloys Compd.* **2007**, *444*, 325–328.
- (105) Ankudinov, A. L.; Ravel, B.; Rehr, J. J.; Conradson, S. D. Real-Space Multiple-Scattering Calculation and Interpretation of X-Ray-Absorption Near-Edge Structure. *Phys. Rev. B* **1998**, *58*, 7565–7576.
- (106) Plateau, C.; Bruckel, P.; Ravat, B.; Delaunay, F. PDF Analysis of PuAl Alloys Local Structure. *J. Nucl. Mater.* **2009**, *385*, 108–111.
- (107) Hess, N. J.; Weber, W. J.; Conradson, S. D. X-Ray Absorption Fine Structure of Aged, Pu-Doped Glass and Ceramic Waste Forms. *J. Nucl. Mater.* **1998**, *254*, 175–184.
- (108) Tyson, T. A.; deLeon, J. M.; Conradson, S. D.; Bishop, A. R.; Neumeier, J. J.; Roder, H.; Zang, J. Evidence for a local lattice distortion in Ca-doped LaMnO<sub>3</sub>. *Phys. Rev. B* **1996**, *53*, 13985–13988.
- (109) Conradson, S. D.; Manara, D.; Wastin, F.; Clark, D. L.; Lander, G. H.; Morales, L. A.; Rebizant, J.; Rondinella, V. V. Local Structure and Charge Distribution in the UO<sub>2</sub>-U<sub>4</sub>O<sub>9</sub> System. *Inorg. Chem.* **2004**, *43*, 6922–6935.
- (110) Faure, P.; Deslandes, B.; Bazin, D.; Tailland, C.; Doukhan, R.; Fournier, J. M.; Falanga, A. Lattice Collapse Around Gallium in PuGa Alloys as Revealed By X-Ray Absorption Spectroscopy. *J. Alloys Compd.* **1996**, *244*, 131–139.
- (111) Nelson, E. J.; Blobaum, J. M.; Wall, M. A.; Allen, P. G.; Schwartz, A. J.; Booth, C. H. Local Structure and Vibrational Properties of alpha'-Pu Martensite and Ga-Stabilized delta-Pu. *AIP Conf. Proc.* **2003**, 187–189.
- (112) Mustre de Leon, J.; Conradson, S. D.; Batistic, I.; Bishop, A. R.; Raistrick, I. D.; Aronson, M. C.; Garzon, F. H. Axial Oxygen-Centered Lattice Instabilities in YBa<sub>2</sub>Cu<sub>3</sub>O<sub>7</sub>: An Application Of the Analysis of Extended X-Ray-Absorption Fine Structure in Anharmonic Systems. *Phys. Rev. B* **1992**, *45*, 2447–2457.
- (113) Migliori, A.; Freibert, F.; Lashley, J. C.; Lawson, A. C.; Baiardo, J. P.; Miller, D. A. Thermodynamics and the Elastic Moduli of Pu. *J. Supercond.* **2002**, *15*, 499–503.
- (114) Migliori, A.; Ledbetter, H.; Lawson, A. C.; Ramirez, A. P.; Miller, D. A.; Betts, J. B.; Ramos, M.; Lashley, J. C. Unexpected Elastic Softening in Delta-Plutonium. *Phys. Rev. B* **2006**, *73*, 052101.
- (115) Migliori, A.; Mihut, A.; Betts, J. B.; Ramos, M.; Mielke, C.; Pantea, C.; Miller, D. A.; Mihut, I. Temperature and Time-Dependence of the Elastic Moduli of Pu and Pu-Ga Alloys. *J. Alloys Compd.* **2007**, *444*, 133–137.
- (116) Nelson, E. J.; Allen, P. G.; Blobaum, K. J. M.; Wall, M. A.; Booth, C. H. Local Structure and Vibrational Properties of alpha-Pu, alpha-U, and the alpha-U Charge-Density Wave. *Phys. Rev. B* **2005**, *71*, 184113.
- (117) Nadykto, B. A. Instability of the Electronic Structure of Actinides Under the High Pressure. *J. Alloys Compd.* **2007**, *444*, 145–148.
- (118) Espinosa, F. J.; Villegas, P.; Lashley, J. C.; Conradson, S. D.; Cox, L. E.; Martinez, R.; Martinez, B.; Morales, L.; Terry, J.; Pereyra, R. A. Local Atomic Structure of alpha-Pu. *Phys. Rev. B* **2001**, *63*, 174111.
- (119) Curro, N. J. Nuclear Magnetic Resonance Studies of delta-Stabilized Plutonium. *Mater. Res. Soc. Symp. Proc.* **2003**, *802*, 53–58.
- (120) Fluss, M. J.; Wirth, B. D.; Wall, M. A.; Felter, T. E.; Caturia, M. J.; Kubota, A.; de la Rubia, T. D. Temperature-Dependent Defect Properties From Ion-Irradiation in Pu(Ga). *J. Alloys Compd.* **2004**, *368*, 62–74.
- (121) Begg, B. D.; Hess, N. J.; Weber, W. J.; Conradson, S. D.; Schweiger, M. J.; Ewing, R. C. XAS and XRD Study of Annealed Pu-238- and Pu-239-Substituted Zircons (Zr<sub>0.92</sub>Pu<sub>0.08</sub>SiO<sub>4</sub>). *J. Nucl. Mater.* **2000**, *278*, 212–224.
- (122) Bouchet, J.; Albers, R. C.; Jones, M. D.; Jornard, G. New Pseudophase Structure for alpha-Pu. *Phys. Rev. Lett.* **2004**, *92*, 095503/1–4.
- (123) Zocco, T. G.; Schwartz, A. J. A Brief History of TEM Observations of Plutonium and its Alloys. *JOM* **2003**, *55*, 24–27.
- (124) Arsenlis, A.; Wolfer, W. G.; Schwartz, A. J. Change in Flow Stress and Ductility of delta-Phase Pu-Ga Alloys Due to Self-Irradiation Damage. *J. Nucl. Mater.* **2005**, *336*, 31–39.

- (125) Schwartz, A. J.; Wall, M. A.; Zocco, T. G.; Wolfer, W. G. Characterization and Modelling of Helium Bubbles in Self-Irradiated Plutonium Alloys. *Philos. Mag.* **2005**, *85*, 479–488.
- (126) Arsenlis, A.; Wirth, B. D.; Rhee, M. Dislocation Density-Based Constitutive Model for the Mechanical Behaviour of Irradiated Cu. *Philos. Mag.* **2004**, *84*, 3617–3635.
- (127) Frauenfelder, H. Proteins: A Challenging Many-Body Problem. *Philos. Mag. B* **1996**, *74*, 579–585.
- (128) Becker, J. D.; Wills, J. M.; Cox, L. E.; Cooper, B. R. Calculated Lattice Relaxation in Pu-Ga. *Phys. Rev. B* **1998**, *58*, 5143–5145.
- (129) Soderlind, P. Ambient Pressure Phase Diagram of Plutonium: A Unified Theory for alpha-Pu and delta-Pu. *Europhys. Lett.* **2001**, *55*, 525–531.
- (130) Soderlind, P.; Landa, A.; Sadigh, B. Density-Functional Investigation of Magnetism in delta-Pu. *Phys. Rev. B* **2002**, *66*, 205109.
- (131) Joyce, J. J.; Wills, J. M.; Durakiewicz, T.; Butterfield, M. T.; Guziewicz, E.; Sarrao, J. L.; Morales, L. A.; Arko, A. J.; Eriksson, O. Photoemission and the Electronic Structure of PuCoGa<sub>5</sub>. *Phys. Rev. Lett.* **2003**, *91*, 17640/1–4.
- (132) Harrison, W. A. Understanding the Phonon Spectrum of Plutonium. *Phys. Rev. B* **2004**, *69*, 113106.
- (133) Harrison, W. A. Theory of the Thermal Properties of delta-Plutonium. *Phys. Rev. B* **2004**, *69*, 224109.
- (134) Landa, A.; Soderlind, P. First-Principles Calculations of Stability of delta-Pu-Am Alloys. *J. Alloys Compd.* **2004**, *376*, 62–67.
- (135) Moore, K. T.; Wall, M. A.; Schwartz, A. J.; Chung, B. W.; Morton, S. A.; Tobin, J. G.; Lazar, J. G.; Tichelaar, F. D.; Zandbergen, H. W.; Soderlind, P.; et al. Electron-Energy-Loss Spectroscopy and X-Ray Absorption Spectroscopy as Complementary Probes for Complex f-Electron Metals: Cerium and Plutonium. *Philos. Mag.* **2004**, *84*, 1039–1056.
- (136) Soderlind, P.; Landa, A.; Sadigh, B.; Vitos, L.; Ruban, A. First-Principles Elastic Constants and Phonons of delta-Pu. *Phys. Rev. B* **2004**, *70*, 144103.
- (137) Baskes, M. I.; Lawson, A. C.; Valone, S. M. Lattice Vibrations in delta-Plutonium: Molecular Dynamics Calculation. *Phys. Rev. B* **2005**, *72*, 014129.
- (138) Boulet, P.; Colineau, E.; Wastin, F.; Javorsky, P.; Griveau, J. C.; Rebizant, J.; Stewart, G. R.; Bauer, E. D. Magnetic Properties of the Two Allotropic Phases of PuGa<sub>3</sub>. *Phys. Rev. B* **2005**, *72*, 064438.
- (139) Gouder, T.; Havela, L.; Rebizant, J. Photoemission Study of delta-Pu with Am Doping. *Physica B* **2005**, *359*, 1090–1092.
- (140) Robert, G.; Pasturel, A.; Siberchicot, B. Vacancy Formation in delta-Plutonium: A Density-Functional Study in the Generalized Gradient Approximation. *Europhys. Lett.* **2005**, *71*, 412–417.
- (141) Siethoff, H. Elastic and Thermal Properties of delta-Plutonium. *Phys. Status Solidi B* **2005**, *242*, 1606–1609.